

On spectral embedding performance and elucidating network structure in stochastic block model graphs

Joshua Cape and Minh Tang and Carey E. Priebe
Department of Applied Mathematics and Statistics
Johns Hopkins University

August 16, 2018

Abstract

Statistical inference on graphs often proceeds via spectral methods involving low-dimensional embeddings of matrix-valued graph representations, such as the graph Laplacian or adjacency matrix. In this paper, we analyze the asymptotic information-theoretic relative performance of Laplacian spectral embedding and adjacency spectral embedding for block assignment recovery in stochastic block model graphs by way of Chernoff information. We investigate the relationship between spectral embedding performance and underlying network structure (e.g. homogeneity, affinity, core-periphery, (un)balancedness) via a comprehensive treatment of the two-block stochastic block model and the class of K -block models exhibiting homogeneous balanced affinity structure. Our findings support the claim that, for a particular notion of sparsity, loosely speaking, “Laplacian spectral embedding favors relatively sparse graphs, whereas adjacency spectral embedding favors not-too-sparse graphs.” We also provide evidence in support of the claim that “adjacency spectral embedding favors core-periphery network structure.”

2010 Mathematics Subject Classification: Primary 62H30; Secondary 62B10.

Keywords: Statistical network analysis; random graphs; stochastic block model; Laplacian spectral embedding; adjacency spectral embedding; Chernoff information; vertex clustering.

1 Preface

The stochastic block model (SBM) (Holland et al., 1983) is a simple yet ubiquitous network model capable of capturing community structure that has been widely studied via spectral methods in the mathematics, statistics, physics, and engineering communities. Each vertex in an n -vertex K -block SBM graph belongs to one of the K blocks (communities), and the probability of any two vertices sharing an edge depends exclusively on the vertices' block assignments (memberships).

This paper provides a detailed comparison of two popular spectral embedding procedures by synthesizing recent advances in random graph limit theory. We undertake an extensive investigation of network structure for stochastic block model graphs by considering sub-models exhibiting various functional relationships, symmetries, and geometric properties within the inherent parameter space consisting of block membership probabilities and block edge probabilities. We also provide a collection of figures depicting relative spectral embedding performance as a function of the SBM parameter space for a range of sub-models exhibiting different forms of network structure, specifically homogeneous community structure, affinity structure, core-periphery structure, and (un)balanced block sizes (see Section 5).

The rest of this paper is organized as follows.

- Section 2 introduces the formal setting considered in this paper and contextualizes this work with respect to the existing statistical network analysis literature.
- Section 3 establishes notation, presents the generalized random dot product graph model of which the stochastic block model is a special case, defines the adjacency and Laplacian spectral embeddings, presents the corresponding spectral embedding limit theorems, and specifies the notion of sparsity considered in this paper.
- Section 4 motivates and formulates a measure of large-sample relative spectral embedding performance via Chernoff information.
- Section 5 presents a treatment of the two-block SBM and certain K -block SBMs

whereby we elucidate the relationship between spectral embedding performance and network model structure.

- Section 6 offers further discussion and some concluding remarks.
- Section 7 provides additional details intended to supplement the main body of this paper.

2 Introduction

Formally, we consider the following stochastic block model setting.

Definition 1 (K -block stochastic block model (SBM)). Let $K \geq 2$ be a positive integer and $\boldsymbol{\pi}$ be a vector in the interior of the $(K - 1)$ -dimensional unit simplex in \mathbb{R}^K . Let $\mathbf{B} \in (0, 1)^{K \times K}$ be a symmetric matrix with distinct rows. We say $(\mathbf{A}, \boldsymbol{\tau}) \sim \text{SBM}(\mathbf{B}, \boldsymbol{\pi})$ with scaling factor $0 < \rho_n \leq 1$ provided the following conditions hold. Firstly, $\boldsymbol{\tau} \equiv (\tau_1, \dots, \tau_n)$ where τ_i are independent and identically distributed (i.i.d.) random variables with $\mathbb{P}[\tau_i = k] = \pi_k$. Then, $\mathbf{A} \in \{0, 1\}^{n \times n}$ denotes a symmetric (adjacency) matrix such that, conditioned on $\boldsymbol{\tau}$, for all $i \leq j$, the entries \mathbf{A}_{ij} are independent Bernoulli random variables with $\mathbb{E}[\mathbf{A}_{ij}] = \rho_n \mathbf{B}_{\tau_i, \tau_j}$. If only \mathbf{A} is observed, namely if $\boldsymbol{\tau}$ is integrated out from $(\mathbf{A}, \boldsymbol{\tau})$, then we write $\mathbf{A} \sim \text{SBM}(\mathbf{B}, \boldsymbol{\pi})$.¹ ▲

The SBM is an example of an inhomogeneous Erdős–Rényi random graph model (Bollobás et al., 2007) and reduces to the classical Erdős–Rényi model (Erdős and Rényi, 1959) in the degenerate case when all the entries of \mathbf{B} are identical. This model enjoys an extensive body of literature focused on spectral methods (von Luxburg, 2007) for statistical estima-

¹The distinct row assumption removes potential redundancy with respect to block connectivity and labeling. Namely, if rows k and k' of \mathbf{B}' are identical, then their corresponding blocks are indistinguishable and can without loss of generality be merged to form a reduced block edge probability matrix \mathbf{B} with corresponding combined block membership probability $\pi_k + \pi_{k'}$. We also remark that Definition 1 implicitly permits vertex self-loops, a choice that we make for mathematical expediency. Whether or not self-loops are disallowed does not alter the asymptotic results and conclusions presented here.

tion, inference, and community detection, including [Fishkind et al. \(2013\)](#); [Lei and Rinaldo \(2015\)](#); [McSherry \(2001\)](#); [Rohe et al. \(2011\)](#); [Sarkar and Bickel \(2015\)](#); [Sussman et al. \(2014\)](#). Considerable effort has also been devoted to the information-theoretic and computational investigation of the SBM as a result of interest in the community detection problem; for an overview see [Abbe \(2018\)](#). Popular variants of the SBM include the mixed-membership stochastic block model ([Airoldi et al., 2008](#)) and the degree-corrected stochastic block model ([Karrer and Newman, 2011](#)).

Within the statistics literature, substantial attention has been paid to the class of K -block SBMs with positive semidefinite block edge probability matrices \mathbf{B} . This is due in part to the extensive study of the *random dot product graph* (RDPG) model ([Athreya et al., 2018](#); [Nickel, 2006](#); [Young and Scheinerman, 2007](#)), a latent position random graph model ([Hoff et al., 2002](#)) which includes positive semidefinite SBMs as a special case. Notably, it was recently shown that for the random dot product graph model, both Laplacian spectral embedding (LSE; see [Definition 3](#)) and adjacency spectral embedding (ASE; see [Definition 3](#)) behave approximately as random samples from Gaussian mixture models ([Athreya et al., 2016](#); [Tang and Priebe, 2016](#)). In tandem with these limit results, the concept of Chernoff information ([Chernoff, 1952](#)) was employed in [Tang and Priebe \(2016\)](#) to demonstrate that neither Laplacian nor adjacency spectral embedding dominates the other for subsequent inference as a spectral embedding method when the underlying inference task is to recover vertices' latent block assignments. In doing so, the results in [Tang and Priebe \(2016\)](#) clarify and complete the groundbreaking work in [Sarkar and Bickel \(2015\)](#) on comparing spectral clusterings for stochastic block model graphs.

In [Tang and Priebe \(2016\)](#) the authors leave open the problem of comprehensively investigating Chernoff information as a measure of relative spectral embedding performance for stochastic block model graphs. Moreover, they do not investigate how relative spectral embedding performance corresponds to underlying network model structure. This is understandable, since the positive semidefinite restriction on \mathbf{B} limits the possible network structure that can be investigated under the random dot product graph model.

More recently, the limit theory in [Tang and Priebe \(2016\)](#) was extended in [Rubin-Delanchy et al. \(2017\)](#) to hold for *all* SBMs within the more flexible framework of the *generalized random dot product graph* (GRDPG) *model*. These developments now make it possible to conduct a more comprehensive Chernoff-based analysis, and that is precisely the aim of this paper. We set forth to formulate and analyze a criterion based on Chernoff information for quantifying relative spectral embedding performance which we then further consider in conjunction with underlying network model structure. The investigation carried out in this paper is, to the best of our knowledge, among the first of its kind in the study of statistical network analysis and random graph inference.

This paper focuses on the following two models which have garnered widespread interest (e.g. see [Abbe \(2018\)](#) and the references therein).

1. The two-block SBM with $\mathbf{B} = \begin{bmatrix} a & b \\ b & c \end{bmatrix}$ and $\boldsymbol{\pi} = (\pi_1, 1 - \pi_1)$ where $a, b, c, \pi_1 \in (0, 1)$;
2. The $K \geq 2$ block SBM exhibiting homogeneous balanced affinity structure, i.e. $\mathbf{B}_{ij} = a$ for all $i = j$, $\mathbf{B}_{ij} = b$ for all $i \neq j$, $0 < b < a < 1$, and $\boldsymbol{\pi} = (\frac{1}{K}, \dots, \frac{1}{K}) \in \mathbb{R}^K$.

Using the concept of Chernoff information (Section 4), we obtain an information-theoretic summary characteristic $\rho^* \equiv \rho^*(\mathbf{B}, \boldsymbol{\pi})$ such that the cases $\rho^* > 1$, $\rho^* < 1$, and $\rho^* = 1$ correspond to the preference of spectral embedding procedure based on approximate large-sample relative performance, summarized as ASE > LSE, ASE < LSE, and ASE = LSE, respectively. The above models' low-dimensional parameter spaces facilitate visualizing and analyzing the relationship between network structure (i.e. SBM($\mathbf{B}, \boldsymbol{\pi}$)) and embedding performance (i.e. $\rho^*(\mathbf{B}, \boldsymbol{\pi})$).

This paper considers the task of performing inference on a single large graph. As such, we interpret the notion of *sparsity* in reference to the magnitudes of probability parameters, namely the magnitudes of the entries of \mathbf{B} . This notion of sparsity corresponds to the interpretation and intuition of a practitioner wanting to do statistics with an observed graph. We shall, with this understanding in mind, subsequently demonstrate that LSE is preferred as an embedding method in relatively sparse regimes, whereas ASE is preferred as an embedding method in not-too-sparse regimes.

By way of contrast, the scaling factor ρ_n in Definition 1, which is included for the purpose of general presentation, indexes a sequence of models wherein edge probabilities change with n . We take ρ_n to be constant in n which by rescaling is equivalent to setting $\rho_n \equiv 1$. Limit theorems are known for regimes where $\rho_n \rightarrow 0$ as $n \rightarrow \infty$, but these regimes are uninteresting for single graph inference from the perspective of relative spectral embedding performance (Tang and Priebe, 2016).

3 Preliminaries

3.1 Notation

In this paper, all vectors and matrices are real-valued. The symbols $:=$ and \equiv are used to assign definitions and to denote formal equivalence, respectively. Given a symmetric positive definite $n \times n$ matrix \mathbf{M} , let $\langle \cdot, \cdot \rangle_{\mathbf{M}} : \mathbb{R}^n \times \mathbb{R}^n \rightarrow \mathbb{R}$ denote the real inner product induced by \mathbf{M} . Similarly, define the induced norm as $\| \cdot \|_{\mathbf{M}} := \sqrt{\langle \cdot, \cdot \rangle_{\mathbf{M}}}$. In particular, given the $n \times n$ identity matrix \mathbf{I} , denote the standard Euclidean inner product and Euclidean norm by $\langle \cdot, \cdot \rangle \equiv \langle \cdot, \cdot \rangle_{\mathbf{I}}$ and $\| \cdot \|_2 := \sqrt{\langle \cdot, \cdot \rangle}$, respectively. Given an underlying matrix, $\det(\cdot)$ and $\text{tr}(\cdot)$ denote the matrix determinant and matrix trace operator, respectively. Given a diagonal matrix $\mathbf{D} := \text{diag}(d_{11}, d_{22}, \dots, d_{nn}) \in \mathbb{R}^{n \times n}$, $|\mathbf{D}|$ denotes the entrywise absolute value (matrix) of \mathbf{D} .

The vector of all ones in \mathbb{R}^n is denoted by $\mathbf{1}_n$, whereas the zero matrix in $\mathbb{R}^{m \times n}$ is denoted by $\mathbf{0}_{m,n}$. We suppress the indices for convenience when the underlying dimensions are understood, writing instead $\mathbf{1}$ and $\mathbf{0}$.

Let $\mathbb{N} := \{1, 2, 3, \dots\}$ denote the set of natural numbers so that for $n \in \mathbb{N}$, $[n] := \{1, 2, \dots, n\}$. For integers $d^+ \geq 1$, $d^- \geq 0$, and $d := d^+ + d^- \geq 1$, let $\mathbf{I}_{d^-}^{d^+} := \mathbf{I}_{d^+} \oplus (-\mathbf{I}_{d^-}) \in \mathbb{R}^{d \times d}$ be the direct sum (diagonal) matrix with identity matrices $\mathbf{I}_{d^+} \in \mathbb{R}^{d^+ \times d^+}$ and $\mathbf{I}_{d^-} \in \mathbb{R}^{d^- \times d^-}$ together with the convention that $\mathbf{I}_0^{d^+} \equiv \mathbf{I}_{d^+}$. For example, $\mathbf{I}_1^1 \equiv \text{diag}(1, -1) \in \mathbb{R}^{2 \times 2}$.

For integers $n \geq d \geq 1$, the set of all $n \times d$ real matrices with orthonormal columns shall

be denoted by $\mathbb{O}_{n,d}$. Let $\mathbb{O}(d^+, d^-)$ denote the indefinite orthogonal group with signature (d^+, d^-) , and let $\mathbb{O}_{d^+} \equiv \mathbb{O}_{d^+, d^+} \equiv \mathbb{O}(d^+, 0)$ denote the orthogonal group in $\mathbb{R}^{d^+ \times d^+}$. In particular, $\mathbf{M} \in \mathbb{O}(d^+, d^-)$ has the characterization $\mathbf{M}^\top \mathbf{I}_{d^-}^{d^+} \mathbf{M} = \mathbf{I}_{d^-}^{d^+}$. In the case of the orthogonal group, this characterization reduces to the relationship $\mathbf{M}^\top \equiv \mathbf{M}^{-1}$.

3.2 The generalized random dot product graph model

A growing corpus has emerged within the statistics literature focused on the development of theory and applications for the *random dot product graph* (RDPG) *model* (Nickel, 2006; Young and Scheinerman, 2007). This latent position random graph model associates to each vertex in a graph an underlying low-dimensional vector. These vectors may be viewed as encoding structural information or attributes possessed by their corresponding vertices. In turn, the probability of two vertices sharing an edge is specified through the standard Euclidean inner (dot) product of the vertices' latent position vectors. While simple in concept and design, this model has proven successful in real-world applications in the areas of neuroscience and social networks (Lyzinski et al., 2017). On the theoretical side, the RDPG model enjoys some of the first-ever statistical theory for two-sample hypothesis testing on random graphs, both semiparametric (Tang et al., 2017) and nonparametric (Tang et al., 2017). For more on the RDPG model, see the survey Athreya et al. (2018) and the references therein.

More recently, the *generalized random dot product graph* (GRDPG) *model* was introduced as an extension of the RDPG model that includes as special cases the mixed membership stochastic block model as well as *all* (single membership) stochastic block models (Rubin-Delanchy et al., 2017). Effort towards the development of theory for the GRDPG model has already raised new questions and produced new findings related to the geometry of spectral methods, embeddings, and random graph inference. The present paper further contributes to these efforts.

Definition 2 (The generalized random dot product graph (GRDPG) model). For integers $d^+ \geq 1$ and $d^- \geq 0$ such that $d := d^+ + d^- \geq 1$, let F be a distribution on a set $\mathcal{X} \subset \mathbb{R}^d$ such that $\langle \mathbf{I}_{d^-}^{d^+} x, y \rangle \in [0, 1]$ for all $x, y \in \mathcal{X}$. We say that $(\mathbf{X}, \mathbf{A}) \sim \text{GRDPG}(F)$ with

signature (d^+, d^-) and scaling factor $0 < \rho_n \leq 1$ if the following hold. Let $X_1, \dots, X_n \sim F$ be independent and identically distributed random (latent position) vectors with

$$\mathbf{X} := [X_1 | \dots | X_n]^\top \in \mathbb{R}^{n \times d} \text{ and } \mathbf{P} := \rho_n \mathbf{X} \mathbf{I}_{d^-}^{d^+} \mathbf{X}^\top \in [0, 1]^{n \times n}. \quad (1)$$

For each $i \leq j$, the entries \mathbf{A}_{ij} of the symmetric adjacency matrix $\mathbf{A} \in \{0, 1\}^{n \times n}$ are then generated in a conditionally independent fashion given the latent positions, namely

$$\{\mathbf{A}_{ij} | X_i, X_j\} \sim \text{Bernoulli}(\rho_n \langle \mathbf{I}_{d^-}^{d^+} X_i, X_j \rangle). \quad (2)$$

In this setting, the conditional probability $\mathbb{P}[\mathbf{A} | \mathbf{X}]$ can be computed explicitly as a product of Bernoulli probabilities. ▲

To reiterate, we consider the regime $\rho_n \equiv 1$ and therefore suppress dependencies on ρ_n later in the text. When no confusion can arise, we also use adorned versions of the symbol ρ to denote Chernoff-related quantities unrelated to ρ_n in a manner consistent with the notation in [Tang and Priebe \(2016\)](#) (see Section 4).

When $d^- = 0$, the GRDPG model reduces to the RDPG model. When the distribution F is a discrete distribution on a finite collection of vectors in \mathbb{R}^d , then the GRDPG model coincides with the SBM, in which case the $n \times n$ edge probability matrix \mathbf{P} arises as an appropriate dilation of the $K \times K$ block edge probability matrix \mathbf{B} . Given any valid $\mathbf{B} \in (0, 1)^{K \times K}$ as in Definition 1, there exist integers d^+, d^- , and a matrix $\mathbf{X} \in \mathbb{R}^{K \times K}$ such that \mathbf{B} has the (not necessarily unique) factorization $\mathbf{B} \equiv \mathbf{X} \mathbf{I}_{d^-}^{d^+} \mathbf{X}^\top$, which follows since the spectral decomposition of \mathbf{B} can be written as $\mathbf{B} \equiv \mathbf{U}_B \mathbf{\Lambda} \mathbf{U}_B^\top = (\mathbf{U}_B |\mathbf{\Lambda}|^{1/2}) \mathbf{I}_{d^-}^{d^+} (\mathbf{U}_B |\mathbf{\Lambda}|^{1/2})^\top$. This demonstrates the ability of the GRDPG framework in Definition 2 to model all possible stochastic block models formulated in Definition 1.

Remark 1 (Non-identifiability in the GRDPG model). The GRDPG model possess two intrinsic sources of non-identifiability, summarized as “uniqueness up to indefinite orthogonal transformations” and “uniqueness up to artificial dimension blow-up”. More precisely, for $(\mathbf{X}, \mathbf{A}) \sim \text{GRDPG}(F)$ with signature (d^+, d^-) , the following considerations must be taken into account.

1. For any $\mathbf{Q} \in \mathbb{O}(d^+, d^-)$, $(\mathbf{X}, \mathbf{A}) \stackrel{d}{=} (\mathbf{Y}, \mathbf{B})$ whenever $(\mathbf{Y}, \mathbf{B}) \sim \text{GRDPG}(F \circ \mathbf{Q})$, where

$F \circ \mathbf{Q}$ denotes the distribution of the latent position vector $Y = \mathbf{Q}X$ and $\stackrel{d}{=}$ denotes equality in distribution. This source of non-identifiability cannot be mitigated. See Eq. (2).

2. There exists a distribution F' on $\mathbb{R}^{d'}$ for some $d' > d$ such that $(\mathbf{X}, \mathbf{A}) \stackrel{d}{=} (\mathbf{Y}, \mathbf{B})$ where $(\mathbf{Y}, \mathbf{B}) \sim \text{GRDPG}(F')$. This source of non-identifiability can be avoided by assuming, as we do in this paper, that F is non-degenerate in the sense that for $X_1 \sim F$, the second moment matrix $\mathbb{E}[X_1 X_1^\top] \in \mathbb{R}^{d \times d}$ is full rank.

Definition 3 (Adjacency and Laplacian spectral embeddings). Let $\mathbf{A} \in \{0, 1\}^{n \times n}$ be a symmetric adjacency matrix with eigendecomposition $\mathbf{A} \equiv \sum_{i=1}^n \lambda_i u_i u_i^\top$ and with ordered eigenvalues $|\lambda_1| \geq |\lambda_2| \geq \dots \geq |\lambda_n|$ corresponding to orthonormal eigenvectors u_1, u_2, \dots, u_n . Given a positive integer d such that $d \leq n$, let $\mathbf{S}_\mathbf{A} := \text{diag}(\lambda_1, \dots, \lambda_d) \in \mathbb{R}^{d \times d}$ and $\mathbf{U}_\mathbf{A} := [u_1 | \dots | u_d] \in \mathbb{O}_{n,d}$. The *adjacency spectral embedding* (ASE) of \mathbf{A} into \mathbb{R}^d is then defined to be the $n \times d$ matrix $\widehat{\mathbf{X}} := \mathbf{U}_\mathbf{A} |\mathbf{S}_\mathbf{A}|^{1/2}$. The matrix $\widehat{\mathbf{X}}$ serves as a consistent estimator for \mathbf{X} up to indefinite orthogonal transformation as $n \rightarrow \infty$.

Along similar lines, define the normalized Laplacian of \mathbf{A} as

$$\mathcal{L}(\mathbf{A}) := (\text{diag}(\mathbf{A}\mathbf{1}_n))^{-1/2} \mathbf{A} (\text{diag}(\mathbf{A}\mathbf{1}_n))^{-1/2} \in \mathbb{R}^{n \times n} \quad (3)$$

whose eigendecomposition is given by $\mathcal{L}(\mathbf{A}) \equiv \sum_{i=1}^n \tilde{\lambda}_i \tilde{u}_i \tilde{u}_i^\top$ with ordered eigenvalues $|\tilde{\lambda}_1| \geq |\tilde{\lambda}_2| \geq \dots \geq |\tilde{\lambda}_n|$ corresponding to orthonormal eigenvectors $\tilde{u}_1, \tilde{u}_2, \dots, \tilde{u}_n$. Given a positive integer d such that $d \leq n$, let $\tilde{\mathbf{S}}_\mathbf{A} := \text{diag}(\tilde{\lambda}_1, \dots, \tilde{\lambda}_d) \in \mathbb{R}^{d \times d}$ and let $\tilde{\mathbf{U}}_\mathbf{A} := [\tilde{u}_1 | \dots | \tilde{u}_d] \in \mathbb{O}_{n,d}$. The *Laplacian spectral embedding* (LSE) of \mathbf{A} into \mathbb{R}^d is then defined to be the $n \times d$ matrix $\check{\mathbf{X}} := \tilde{\mathbf{U}}_\mathbf{A} |\tilde{\mathbf{S}}_\mathbf{A}|^{1/2}$. The matrix $\check{\mathbf{X}}$ serves as a consistent estimator for the matrix $(\text{diag}(\mathbf{X}\mathbf{I}_d^+ \mathbf{X}^\top \mathbf{1}_n))^{-1/2} \mathbf{X}$ up to indefinite orthogonal transformation as $n \rightarrow \infty$. \blacktriangle

Remark 2 (Consistent estimation and parametrization involving latent positions). The matrices \mathbf{X} and $(\text{diag}(\mathbf{X}\mathbf{I}_d^+ \mathbf{X}^\top \mathbf{1}_n))^{-1/2} \mathbf{X}$, which are one-to-one invertible transformations of each other, may be viewed as providing different parametrizations of GRDPG graphs. As such, comparing $\widehat{\mathbf{X}}$ and $\check{\mathbf{X}}$ as estimators is non-trivial. In order to carry out such a comparison, we subsequently adopt an information-theoretic approach in which we consider a particular choice of f -divergence which is both analytically tractable and statistically

interpretable in the current setting.

For the subsequent purposes of the present work, Theorems 4 and 5 (below) state slightly weaker formulations of the corresponding limit theorems obtained in Rubin-Delanchy et al. (2017) for adjacency and Laplacian spectral embedding.

Theorem 4 (ASE limit theorem for GRDPG, adapted from Rubin-Delanchy et al. (2017)). *Assume the d -dimensional GRDPG setting in Definition 2 with $\rho_n \equiv 1$. Let $\widehat{\mathbf{X}}$ be the adjacency spectral embedding into \mathbb{R}^d with i -th row denoted by \widehat{X}_i . Let $\Phi(\cdot, \Sigma)$ denote the cumulative distribution function of the centered multivariate normal distribution in \mathbb{R}^d with covariance matrix Σ . Then, with respect to the adjacency spectral embedding, there exists a sequence of matrices $\mathbf{Q} \equiv \mathbf{Q}_n \in \mathbb{O}(d^+, d^-)$ such that, for any $z \in \mathbb{R}^d$,*

$$\mathbb{P} \left[\sqrt{n} \left(\mathbf{Q} \widehat{X}_i - X_i \right) \leq z \right] \rightarrow \int_x \Phi(z, \Sigma(x)) dF(x) \quad (4)$$

as $n \rightarrow \infty$, where for $X_1 \sim F$,

$$\Sigma(x) := \mathbf{I}_d^{d+} \Delta^{-1} \mathbb{E} \left[g(x, X_1) X_1 X_1^\top \right] \Delta^{-1} \mathbf{I}_d^{d+},$$

with $\Delta := \mathbb{E}[X_1 X_1^\top]$ and $g(x, X_1) := \langle \mathbf{I}_d^{d+} x, X_1 \rangle (1 - \langle \mathbf{I}_d^{d+} x, X_1 \rangle)$.

Theorem 5 (LSE limit theorem for GRDPG, adapted from Rubin-Delanchy et al. (2017)). *Assume the d -dimensional GRDPG setting in Definition 2 with $\rho_n \equiv 1$. Let $\check{\mathbf{X}}$ be the Laplacian spectral embedding into \mathbb{R}^d with i -th row denoted by \check{X}_i . Let $\Phi(\cdot, \Sigma)$ denote the cumulative distribution function of the centered multivariate normal distribution in \mathbb{R}^d with covariance matrix Σ . Then, with respect to the Laplacian spectral embedding, there exists a sequence of matrices $\tilde{\mathbf{Q}} \equiv \tilde{\mathbf{Q}}_n \in \mathbb{O}(d^+, d^-)$ such that, for any $z \in \mathbb{R}^d$,*

$$\mathbb{P} \left[n \left(\tilde{\mathbf{Q}} \check{X}_i - \frac{X_i}{\sqrt{\sum_j \langle \mathbf{I}_d^{d+} X_i, X_j \rangle}} \right) \leq z \right] \rightarrow \int_x \Phi(z, \tilde{\Sigma}(x)) dF(x) \quad (5)$$

as $n \rightarrow \infty$, where for $X_1 \sim F$ and $\mu := \mathbb{E}[X_1]$,

$$\tilde{\Sigma}(x) := \mathbf{I}_d^{d+} \tilde{\Delta}^{-1} \mathbb{E} \left[\tilde{g}(x, X_1) \left(\frac{X_1}{\langle \mathbf{I}_d^{d+} \mu, X_1 \rangle} - \frac{\tilde{\Delta} \mathbf{I}_d^{d+} x}{2 \langle \mathbf{I}_d^{d+} \mu, x \rangle} \right) \left(\frac{X_1}{\langle \mathbf{I}_d^{d+} \mu, X_1 \rangle} - \frac{\tilde{\Delta} \mathbf{I}_d^{d+} x}{2 \langle \mathbf{I}_d^{d+} \mu, x \rangle} \right)^\top \right] \tilde{\Delta}^{-1} \mathbf{I}_d^{d+},$$

with $\tilde{\Delta} := \mathbb{E} \left[\langle \mathbf{I}_d^{d+} \mu, X_1 \rangle^{-1} X_1 X_1^\top \right]$ and $\tilde{g}(x, X_1) := \left[\langle \mathbf{I}_d^{d+} \mu, x \rangle^{-1} \langle \mathbf{I}_d^{d+} x, X_1 \rangle (1 - \langle \mathbf{I}_d^{d+} x, X_1 \rangle) \right]$.

4 Spectral embedding performance

We desire to compare the large- n sample relative performance of adjacency and Laplacian spectral embedding for subsequent inference, where the subsequent inference task is naturally taken to be the problem of recovering latent block assignments. Here, measuring spectral embedding performance will correspond to estimating the large-sample optimal error rate for recovering the underlying block assignments following each of the spectral embeddings. Towards this end, we now introduce Chernoff information and Chernoff divergence as appropriate information-theoretic quantities.

Given independent and identically distributed random vectors Y_i arising from one of two absolutely continuous multivariate distributions F_1 and F_2 on $\Omega = \mathbb{R}^d$ with density functions f_1 and f_2 , respectively, we are interested in testing the simple null hypothesis $\mathbb{H}_0 : F = F_1$ against the simple alternative hypothesis $\mathbb{H}_A : F = F_2$. In this framework, a statistical test T can be viewed as a sequence of mappings $T_m : \Omega^m \rightarrow \{1, 2\}$ indexed according to sample size m such that T_m returns the value two when \mathbb{H}_0 is rejected in favor of \mathbb{H}_A and correspondingly returns the value one when \mathbb{H}_0 is favored. For each m , the corresponding significance level and type-II error are denoted by α_m and β_m , respectively.

Assume that the prior probability of \mathbb{H}_0 being true is given by $\pi \in (0, 1)$. For a given $\alpha_m^* \in (0, 1)$, let $\beta_m^* \equiv \beta_m^*(\alpha_m^*)$ denote the type-II error associated with the corresponding likelihood ratio test when the type-I error is at most α_m^* . Then, the *Bayes risk* in deciding between \mathbb{H}_0 and \mathbb{H}_A given m independent random vectors Y_1, Y_2, \dots, Y_m is given by

$$\inf_{\alpha_m^* \in (0, 1)} \pi \alpha_m^* + (1 - \pi) \beta_m^*. \quad (6)$$

The Bayes risk is intrinsically related to *Chernoff information* (Chernoff, 1952, 1956), $C(F_1, F_2)$, namely

$$\lim_{m \rightarrow \infty} \frac{1}{m} \left[\inf_{\alpha_m^* \in (0, 1)} \log(\pi \alpha_m^* + (1 - \pi) \beta_m^*) \right] = -C(F_1, F_2), \quad (7)$$

where

$$C(F_1, F_2) := -\log \left[\inf_{t \in (0, 1)} \int_{\mathbb{R}^d} f_1^t(x) f_2^{1-t}(x) dx \right] = \sup_{t \in (0, 1)} \left[-\log \int_{\mathbb{R}^d} f_1^t(x) f_2^{1-t}(x) dx \right].$$

In words, the Chernoff information between F_1 and F_2 is the exponential rate at which the Bayes risk decreases as $m \rightarrow \infty$. Note that the Chernoff information is independent of the prior probability π . A version of Eq. (7) also holds when considering $K \geq 3$ hypothesis with distributions F_1, F_2, \dots, F_K , thereby introducing the quantity $\min_{k \neq l} C(F_k, F_l)$ (see for example Tang and Priebe (2016)).

Chernoff information can be expressed in terms of the *Chernoff divergence* between distributions F_1 and F_2 , defined for $t \in (0, 1)$ as

$$C_t(F_1, F_2) = -\log \int_{\mathbb{R}^d} f_1^t(x) f_2^{1-t}(x) dx, \quad (8)$$

which yields the relation

$$C(F_1, F_2) = \sup_{t \in (0, 1)} C_t(F_1, F_2). \quad (9)$$

The Chernoff divergence is an example of an f -divergence and as such satisfies the data processing lemma (Liese and Vajda, 2006) and is invariant with respect to invertible transformations (Devroye et al., 2013). One could instead use another f -divergence for the purpose of comparing the two embedding methods, such as the Kullback-Liebler divergence. Our choice is motivated by the aforementioned relationship with Bayes risk in Eq. (7).

In this paper we explicitly consider multivariate normal distributions as a consequence of Theorems 4 and 5 when conditioning on the individual underlying latent positions for stochastic block model graphs. In particular, given $F_1 = \mathcal{N}(\mu_1, \Sigma_1)$, $F_2 = \mathcal{N}(\mu_2, \Sigma_2)$, and $t \in (0, 1)$, then for $\Sigma_t := t\Sigma_1 + (1-t)\Sigma_2$, the Chernoff information between F_1 and F_2 is given by

$$\begin{aligned} C(F_1, F_2) &= \sup_{t \in (0, 1)} \left[\frac{t(1-t)}{2} (\mu_2 - \mu_1)^\top \Sigma_t^{-1} (\mu_2 - \mu_1) + \frac{1}{2} \log \left(\frac{\det(\Sigma_t)}{\det(\Sigma_1)^t \det(\Sigma_2)^{1-t}} \right) \right] \\ &= \sup_{t \in (0, 1)} \left[\frac{t(1-t)}{2} \|\mu_2 - \mu_1\|_{\Sigma_t^{-1}}^2 + \frac{1}{2} \log \left(\frac{\det(\Sigma_t)}{\det(\Sigma_1)^t \det(\Sigma_2)^{1-t}} \right) \right]. \end{aligned}$$

Let $\mathbf{B} \in (0, 1)^{K \times K}$ and $\boldsymbol{\pi}$ denote the matrix of block edge probabilities and the vector of block assignment probabilities for a K -block stochastic block model as before. This corresponds to a special case of the GRDPG model with signature (d^+, d^-) , $d^+ + d^- = \text{rank}(\mathbf{B})$, and latent positions $\nu_k \in \mathbb{R}^{\text{rank}(\mathbf{B})}$. For an n -vertex SBM graph with parameters $(\mathbf{B}, \boldsymbol{\pi})$, the

large-sample optimal error rate for recovering block assignments when performing adjacency spectral embedding can be characterized by the quantity $\rho_A \equiv \rho_A(\mathbf{B}, \boldsymbol{\pi}, n)$ defined by

$$\rho_A := \min_{k \neq l} \sup_{t \in (0,1)} \left[\frac{nt(1-t)}{2} \|\nu_k - \nu_l\|_{\boldsymbol{\Sigma}_{kl}^{-1}(t)}^2 + \frac{1}{2} \log \left(\frac{\det(\boldsymbol{\Sigma}_{kl}(t))}{\det(\boldsymbol{\Sigma}_k)^t \det(\boldsymbol{\Sigma}_l)^{1-t}} \right) \right], \quad (10)$$

where $\boldsymbol{\Sigma}_{kl}(t) := t\boldsymbol{\Sigma}_k + (1-t)\boldsymbol{\Sigma}_l$ for $t \in (0, 1)$.

Similarly, for Laplacian spectral embedding, $\rho_L \equiv \rho_L(\mathbf{B}, \boldsymbol{\pi}, n)$, one has

$$\rho_L := \min_{k \neq l} \sup_{t \in (0,1)} \left[\frac{nt(1-t)}{2} \|\tilde{\nu}_k - \tilde{\nu}_l\|_{\tilde{\boldsymbol{\Sigma}}_{kl}^{-1}(t)}^2 + \frac{1}{2} \log \left(\frac{\det(\tilde{\boldsymbol{\Sigma}}_{kl}(t))}{\det(\tilde{\boldsymbol{\Sigma}}_k)^t \det(\tilde{\boldsymbol{\Sigma}}_l)^{1-t}} \right) \right], \quad (11)$$

where $\tilde{\boldsymbol{\Sigma}}_{kl}(t) := t\tilde{\boldsymbol{\Sigma}}_k + (1-t)\tilde{\boldsymbol{\Sigma}}_l$ and $\tilde{\nu}_k := \nu_k / (\sum_{k'} \pi_{k'} \langle \mathbf{I}_{d^-}^{d^+} \nu_{k'}, \nu_k \rangle)^{1/2}$.

The factor n in Eqs. (10–11) arises from the implicit consideration of the appropriate (non-singular) theoretical sample covariance matrices. To assist in the comparison and interpretation of the quantities ρ_A and ρ_L , we assume throughout this paper that $n_k = n\pi_k$ for $\tilde{\nu}_k$. The logarithmic terms in Eqs. (10–11) as well as the deviations of each term n_k from $n\pi_k$ are negligible for large n , collectively motivating the following large-sample measure of relative performance, ρ^* , where

$$\frac{\rho_A}{\rho_L} \equiv \frac{\rho_A(n)}{\rho_L(n)} \rightarrow \rho^* \equiv \frac{\rho_A^*}{\rho_L^*} := \frac{\min_{k \neq l} \sup_{t \in (0,1)} \left[t(1-t) \|\nu_k - \nu_l\|_{\boldsymbol{\Sigma}_{kl}^{-1}(t)}^2 \right]}{\min_{k \neq l} \sup_{t \in (0,1)} \left[t(1-t) \|\tilde{\nu}_k - \tilde{\nu}_l\|_{\tilde{\boldsymbol{\Sigma}}_{kl}^{-1}(t)}^2 \right]}. \quad (12)$$

Here we have suppressed the functional dependence on the underlying model parameters \mathbf{B} and $\boldsymbol{\pi}$. For large n , observe that as ρ_A^* increases, ρ_A also increases, and therefore the large-sample optimal error rate corresponding to adjacency spectral embedding decreases in light of Eq. (7) and its generalization. Similarly, large values of ρ_L^* correspond to good theoretical performance of Laplacian spectral embedding. Thus, if $\rho^* > 1$, then ASE is to be preferred to LSE, whereas if $\rho^* < 1$, then LSE is to be preferred to ASE. The case when $\rho^* = 1$ indicates that neither ASE nor LSE is superior for the given parameters \mathbf{B} and $\boldsymbol{\pi}$. To reiterate, we summarize these preferences as ASE > LSE, ASE < LSE, and ASE = LSE, respectively.

In what follows, we fixate on the asymptotic quantity ρ^* . For the two-block SBM and certain K -block SBMs exhibiting symmetry, Eq. (12) reduces to the simpler form

$$\rho^* = \frac{\sup_{t \in (0,1)} \left[t(1-t) \|\nu_1 - \nu_2\|_{\Sigma_{1,2}^{-1}(t)}^2 \right]}{\sup_{t \in (0,1)} \left[t(1-t) \|\tilde{\nu}_1 - \tilde{\nu}_2\|_{\tilde{\Sigma}_{1,2}^{-1}(t)}^2 \right]} \quad (13)$$

for canonically specified latent positions ν_1 and ν_2 . In some cases it is possible to concisely obtain analytic expressions (in t) for both the numerator and denominator. In other cases this is not possible. A related challenge with respect to Eq. (12) is analytically inverting the interpolated block conditional covariance matrices $\Sigma_{1,2}(t)$ and $\tilde{\Sigma}_{1,2}(t)$. Section 7 provides additional technical details and discussion addressing these issues.

5 Elucidating network structure

5.1 The two-block stochastic block model

Consider the set of two-block SBMs with parameters $\boldsymbol{\pi} \equiv (\pi_1, 1 - \pi_1)$ and $\mathbf{B} \in \mathcal{B} := \left\{ \mathbf{B} = \begin{bmatrix} a & b \\ b & c \end{bmatrix} : a, b, c \in (0, 1) \right\}$. For $\boldsymbol{\pi} = (\frac{1}{2}, \frac{1}{2})$, then $a \geq c$ without loss of generality by symmetry. In general, for any fixed choice of $\boldsymbol{\pi}$, the class of models \mathcal{B} can be partitioned according to matrix rank, namely

$$\mathcal{B} \equiv \mathcal{B}_1 \bigsqcup \mathcal{B}_2 := \{ \mathbf{B} : \text{rank}(\mathbf{B}) = 1; a, b, c \in (0, 1) \} \bigsqcup \{ \mathbf{B} : \text{rank}(\mathbf{B}) = 2; a, b, c \in (0, 1) \}.$$

The collection of sub-models \mathcal{B}_1 further decomposes into the disjoint union of the Erdős–Rényi model with homogeneous edge probability $a = b = c \in (0, 1)$ and its relative complement in \mathcal{B}_1 satisfying the determinant constraint $\det(\mathbf{B}) \equiv ac - b^2 = 0$. These partial sub-models can be viewed as one-dimensional and two-dimensional (parameter) regions in the open unit cube, $(0, 1)^3$, respectively.

Similarly, the collection of sub-models \mathcal{B}_2 further decomposes into the disjoint union of $\text{PD}_2 \cap \mathcal{B}_2$ and $\text{IND}_2 \cap \mathcal{B}_2$, where PD_2 denotes the set of positive definite matrices in $\mathbb{R}^{2 \times 2}$

and $\text{IND}_2 := \{\mathbf{B} \in \mathcal{B}_2 : \exists \mathbf{X} \in \mathbb{R}^{2 \times 2}, \text{rank}(\mathbf{X}) = 2, \mathbf{B} = \mathbf{X} \mathbf{I}_1^1 \mathbf{X}^\top\}$. Here only $\mathbf{I}_0^2 \equiv \mathbf{I}_2$ and \mathbf{I}_1^1 are necessary for computing edge probabilities via inner products of the latent positions. Both of these partial sub-models can be viewed as three-dimensional (parameter) regions in $(0, 1)^3$.

Remark 3 (Latent position parametrization). One might ask whether or not for our purposes there exists a “best” latent position representation for some or even every SBM. To this end and more generally, for any $K \geq 2$ and $\mathbf{M} \in \text{PD}_K \subset \mathbb{R}^{K \times K}$, there exists a unique lower-triangular matrix $\mathbf{L} \in \mathbb{R}^{K \times K}$ with positive diagonal entries such that $\mathbf{M} = \mathbf{L} \mathbf{L}^\top$ by the Cholesky matrix decomposition. This yields a canonical choice for the matrix of latent positions \mathbf{X} when \mathbf{B} is positive definite. In particular, for $\mathbf{B} \in \text{PD}_2$, then $\mathbf{B} = \mathbf{X} \mathbf{I}_2 \mathbf{X}^\top$ with $\mathbf{X} := \begin{bmatrix} \sqrt{a} & 0 \\ b/\sqrt{a} & \sqrt{ac-b^2}/\sqrt{a} \end{bmatrix}$. In contrast, for $\mathbf{B} \in \text{IND}_2$, then $\mathbf{B} = \mathbf{X} \mathbf{I}_1^1 \mathbf{X}^\top$ with $\mathbf{X} := \begin{bmatrix} \sqrt{a} & 0 \\ b/\sqrt{a} & \sqrt{b^2-ac}/\sqrt{a} \end{bmatrix}$, keeping in mind that in this case $b^2 - ac > 0$. The latter factorization may be viewed informally as an indefinite Cholesky decomposition under \mathbf{I}_1^1 . For the collection of rank one sub-models \mathcal{B}_1 , the latent positions ν_1 and ν_2 are simply taken to be scalar-valued.

5.1.1 Homogeneous balanced network structure

We refer to the two-block SBM sub-model with $\mathbf{B} = \begin{bmatrix} a & b \\ b & a \end{bmatrix}$ and $\boldsymbol{\pi} = (\frac{1}{2}, \frac{1}{2})$ as the *homogeneous balanced two-block SBM*. The cases when $a > b$, $a < b$, and $a = b$ correspond to the cases when \mathbf{B} is positive definite, indefinite, and reduces to Erdős–Rényi, respectively. The positive definite parameter regime has the network structure interpretation of being *assortative* in the sense that the within-block edge probability a is larger than the between-block edge probability b , consistent with the affinity-based notion of community structure. In contrast, the indefinite parameter regime has the network structure interpretation of being *disassortative* in the sense that between-block edge density exceeds within-block edge density, consistent with the “opposites attract” notion of community structure.

For this SBM sub-model, ρ^* can be simplified analytically (see Section 7 for additional

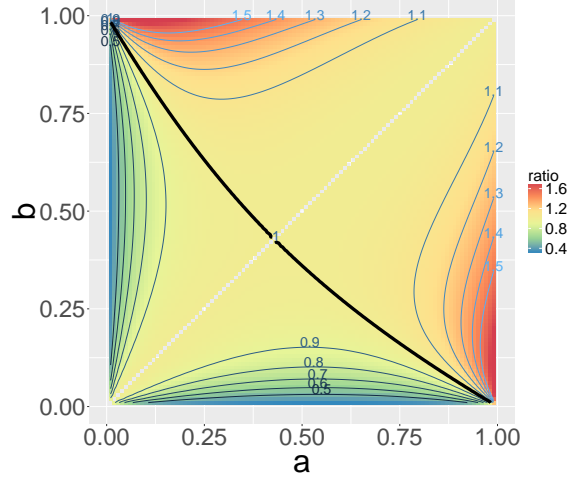


Figure 1: The ratio ρ^* for the homogeneous balanced sub-model in Section 5.1.1. The empty diagonal depicts the Erdős–Rényi model singularity at $a = b$.

details) and can be expressed as a translation with respect to the value one, namely

$$\rho^* \equiv \rho_{a,b}^* = 1 + \frac{(a-b)^2(3a(a-1) + 3b(b-1) + 8ab)}{4(a+b)^2(a(1-a) + b(1-b))} := 1 + c_{a,b} \times \psi_{a,b}, \quad (14)$$

where $\psi_{a,b} := 3a(a-1) + 3b(b-1) + 8ab$ and $c_{a,b} > 0$. By recognizing that $\psi_{a,b}$ functions as a discriminating term, it is straightforward to read off the relative performance of ASE and LSE according to Table 1.

Table 1: Summary of embedding performance in Section 5.1.1

$\rho^* = 1 \iff \psi_{a,b} = 0$; (ASE = LSE)
$\rho^* > 1 \iff \psi_{a,b} > 0$; (ASE > LSE)
$\rho^* < 1 \iff \psi_{a,b} < 0$; (ASE < LSE)

Further investigation of Eq. (14) leads to the observation that $\text{ASE} < \text{LSE}$ for all $0 < b < a \leq \frac{3}{7}$, thereby yielding a parameter region for which LSE dominates ASE. On the other hand, for any fixed $b \in (0, 1)$ there exist values $a_1 < a_2$ such that $\text{ASE} < \text{LSE}$ under a_1 , whereas $\text{ASE} > \text{LSE}$ under a_2 . Figure 1 demonstrates that for homogeneous balanced network structure, LSE is preferred to ASE when the entries in \mathbf{B} are sufficiently small, whereas conversely ASE is preferred to LSE when the entries in \mathbf{B} are not too small.

Remark 4 (Model spectrum and ASE dominance I). In the current setting $\lambda_{\max}(\mathbf{B}) = a + b$, hence $\lambda_{\max}(\mathbf{B}) > 1$ implies ASE $>$ LSE by Eq. (14). This observation amounts to a network structure-based (i.e. \mathbf{B} -based) spectral sufficient condition for determining when ASE is preferred to LSE.

Remark 5 (A balanced one-dimensional SBM restricted sub-model). When $b = 1 - a$, the homogeneous balanced sub-model further reduces to a one-dimensional parameter space such that ρ^* simplifies to

$$\rho^* = 1 + \frac{1}{4}(2a - 1)^2 \geq 1, \quad (15)$$

demonstrating that ASE uniformly dominates LSE for this restricted sub-model. Additionally, it is potentially of interest to note that in this setting the marginal covariance matrices from Theorem 4 for ASE coincide for each block. In contrast, the same behavior is not true for LSE.

5.1.2 Core-periphery network structure

We refer to the two-block SBM sub-model with $\mathbf{B} = \begin{bmatrix} a & b \\ b & b \end{bmatrix}$ and $\boldsymbol{\pi} = (\pi_1, 1 - \pi_1)$ as the *core-periphery two-block SBM*. We explicitly consider the balanced (block size) regime in which $\boldsymbol{\pi} = (\frac{1}{2}, \frac{1}{2})$ and an unbalanced regime in which $\boldsymbol{\pi} = (\frac{1}{4}, \frac{3}{4})$. Here, the cases $a > b$, $a < b$, and $a = b$ correspond to the cases when \mathbf{B} is positive definite, indefinite, and reduces to the Erdős–Rényi model, respectively.

For this sub-model, the ratio ρ^* is not analytically tractable in general. That is to say, simple closed-form solutions do not simultaneously exist for the numerator and denominator in the definition of ρ^* . As such, Figure 2 is obtained numerically by evaluating ρ^* on a grid of points in $(0, 1)^2$ followed by smoothing.

For $a > b$, graphs generated from this SBM sub-model exhibit the popular interpretation of core-periphery structure in which vertices forming a dense core are attached to surrounding periphery vertices with comparatively smaller edge connectivity. Provided the core is sufficiently dense, namely for $a > \frac{1}{4}$ in the balanced regime and $a > \frac{1}{2}$ in the unbalanced regime,

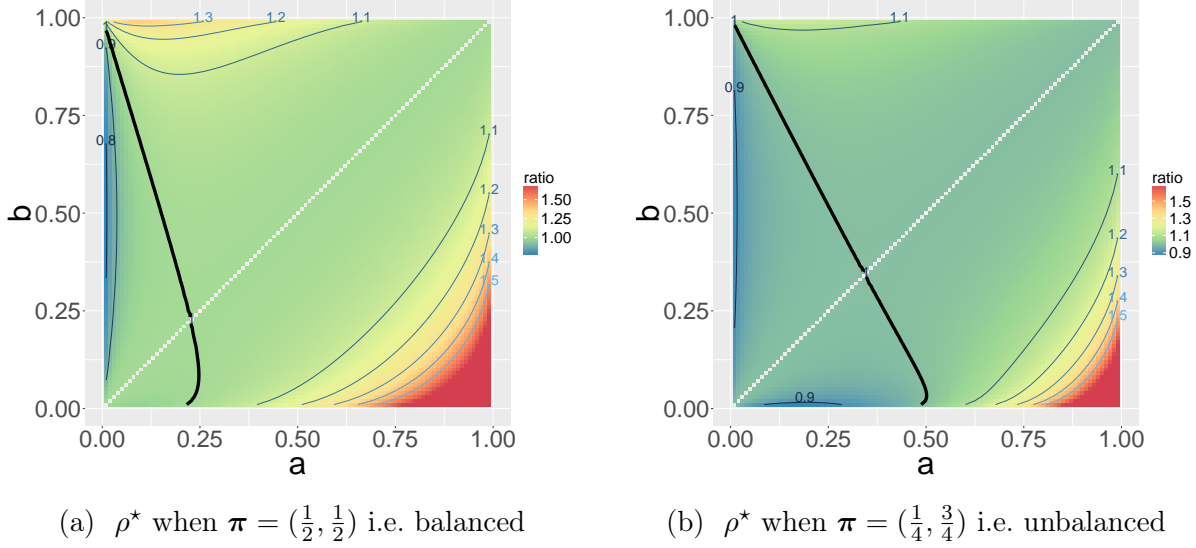


Figure 2: The ratio ρ^* for the core-periphery sub-model in Section 5.1.2. The empty diagonal depicts the Erdős–Rényi model singularity at $a = b$.

Figure 2 demonstrates that $\text{ASE} > \text{LSE}$. Conversely, $\text{ASE} < \text{LSE}$ uniformly in $0 < b < a$ for small enough values of a in both the balanced and unbalanced regime.

In contrast, when $a < b$, the sub-model produces graphs whose network structure is interpreted as having a comparatively sparse induced subgraph which is strongly connected to all vertices in the graph but for which the subgraph vertices exhibit comparatively weaker connectivity. Alternatively, the second block may itself be viewed as a dense core which is simultaneously densely connected to all vertices in the graph. Figure 2 illustrates that for the balanced regime, LSE is preferred for sparser induced subgraphs. Put differently, for large enough dense core with dense periphery, then ASE is the preferable spectral embedding procedure. LSE is preferred to ASE in only a relatively small region corresponding approximately to the triangular region where $0 < b < 1 - 4a$, which as a subset of the unit square has area $\frac{1}{8}$. Similar behavior holds for the unbalanced regime for approximately the (enlarged) triangular region of the parameter space where $0 < b < 1 - 2a$, which as a subset of the unit square has area $\frac{1}{4}$.

Figure 2 suggests that as π_1 decreases from $\frac{1}{2}$ to $\frac{1}{4}$, LSE is favored in a growing region of the

parameter space, albeit still in a smaller region than that for which ASE is to be preferred. Together with the observation that LSE dominates in the lower-left corner of the plots in Figure 2 where a and b have small magnitude, we are led to say in summary that LSE favors relatively sparse core-periphery network structure. To reiterate, sparsity is interpreted with respect to the parameters a and b , keeping in mind the underlying simplifying assumption that $n_k = n\pi_k$ for $k = 1, 2$.

Remark 6 (Model spectrum and ASE dominance II). For $0 < b < a < 1$, then $\lambda_{\max}(\mathbf{B}) = \frac{1}{2}(a + b + \sqrt{a^2 - 2ab + 5b^2})$. Numerical evaluation (not shown) yields that $\lambda_{\max}(\mathbf{B}) > \frac{1}{2}$ implies ASE > LSE. Along the same lines as the discussion in Section 5.1.1, this observation provides a network structure (i.e. \mathbf{B} -based) spectral sufficient condition for this sub-model for determining the relative embedding performance ASE > LSE.

5.1.3 Two-block rank one sub-model

The sub-model for which $\mathbf{B} = \begin{bmatrix} a & b \\ b & c \end{bmatrix}$ with $a, b, c \in (0, 1)$ and $\det(\mathbf{B}) = 0$ can be re-parameterized according to the assignments $a \mapsto p^2$ and $c \mapsto q^2$, yielding $\mathbf{B} = \begin{bmatrix} p^2 & pq \\ pq & q^2 \end{bmatrix}$ with $p, q \in (0, 1)$. Here $\text{rank}(\mathbf{B}) = 1$ and \mathbf{B} is positive semidefinite, corresponding to the one-dimensional RDPG model with latent positions given by the scalars p and q with associated probabilities π_1 and π_2 , respectively. Explicit computation yields the expression

$$\rho^* = \frac{(\sqrt{p} + \sqrt{q})^2(\pi_1 p^2 + \pi_2 q^2)^2 \left(\sqrt{\pi_1 p(1-p^2) + \pi_2 q(1-pq)} + \sqrt{\pi_1 p(1-pq) + \pi_2 q(1-q^2)} \right)^2}{4(\pi_1 p + \pi_2 q)^2 \left(\sqrt{\pi_1 p^4(1-p^2) + \pi_2 pq^3(1-pq)} + \sqrt{\pi_1 p^3 q(1-pq) + \pi_2 q^4(1-q^2)} \right)^2}, \quad (16)$$

whereby ρ^* is given as an explicit, closed-form function of the parameter values p , q , and π_1 with $\pi_2 = 1 - \pi_1$. The simplicity of this sub-model together with its analytic tractability with respect to both \mathbf{B} and $\boldsymbol{\pi}$ makes it particularly amenable to study for the purpose of elucidating network structure. Below, consideration of this sub-model further illustrates the relationship between (parameter-based) sparsity and relative embedding performance.

Figure 3 demonstrates how LSE favors sparse graphs in the sense of the edge probabilities, p and q , as well as how relative performance changes in light of (un)balanced block sizes,

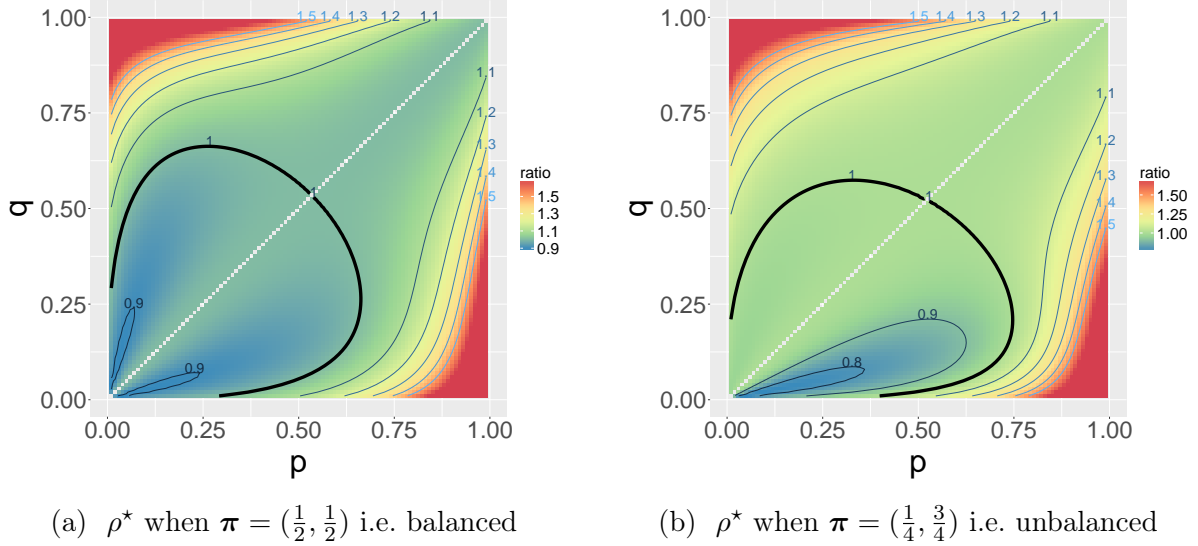


Figure 3: The ratio ρ^* for the two-block rank one sub-model in Section 5.1.3. The empty diagonal depicts the Erdős–Rényi model singularity at $p = q$.

reflected by π_1 . Here the underlying \mathbf{B} matrix is always positive semidefinite, and each of the regions $p > q$ and $p < q$ corresponds to a modified notion of core-periphery structure. For example, when $p > q$, then $\mathbf{B} = \begin{bmatrix} p_1 & p_2 \\ p_2 & p_3 \end{bmatrix}$ with $p_1 > p_2 > p_3$, yielding a hierarchy of core-periphery structure when passing from vertices that are both in block one to vertices that are in different blocks and finally to vertices that are both in block two. Note the similar behavior in the bottom-right triangular regions in Figure 3a–3b and in the same bottom-right triangular region in Figure 2.

Remark 7 (The two-block polynomial p SBM restricted sub-model). Consider the restricted sub-model in which $\mathbf{B} = \begin{bmatrix} p^2 & p^{\gamma+1} \\ p^{\gamma+1} & p^{2\gamma} \end{bmatrix}$, where $\gamma > 1$ and $\pi_1 \in (0, 1)$. For $\gamma \gg 1$ and π_1 fixed, then ρ^* in Eq. (16) satisfies the approximate behavior

$$\rho^* \approx \frac{(1 + \sqrt{1 - p^2})^2}{4(1 - p^2)}. \quad (17)$$

The above approximation exceeds the value one since $1 > \sqrt{1 - p^2}$ for $p \in (0, 1)$ and is simultaneously agnostic with respect to π_1 . Moreover, for large values of γ , the block edge probability matrix is approximately of the form $\mathbf{B} \approx \begin{bmatrix} p_1 & p_2 \\ p_2 & p_3 \end{bmatrix}$ with $p_1 \gg p_2 \approx p_3$, where p_2 and p_3 are very small. This restricted sub-model can therefore be viewed as exhibiting an extremal version of core-periphery structure corresponding to the extremal regions in

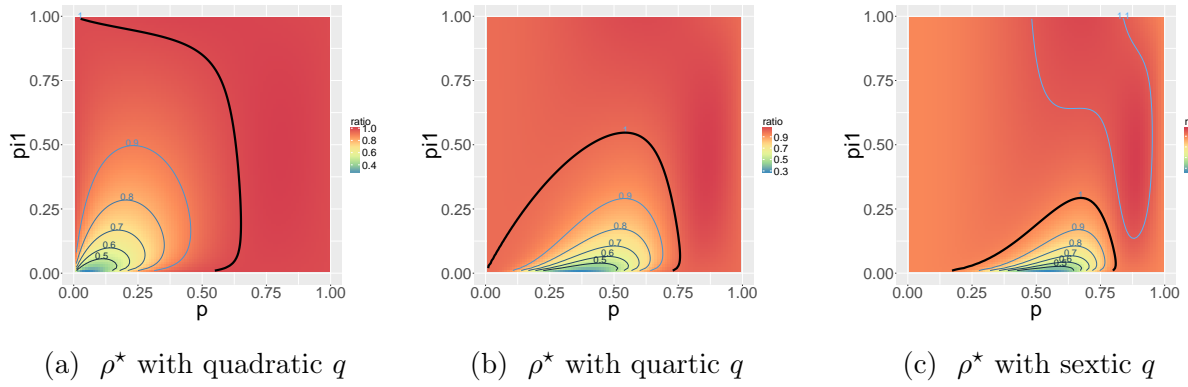


Figure 4: The ratio ρ^* for $p, \pi_1 \in (0, 1)$ when $q = p^\gamma$, $\gamma \in \{2, 4, 6\}$ in Section 5.1.3.

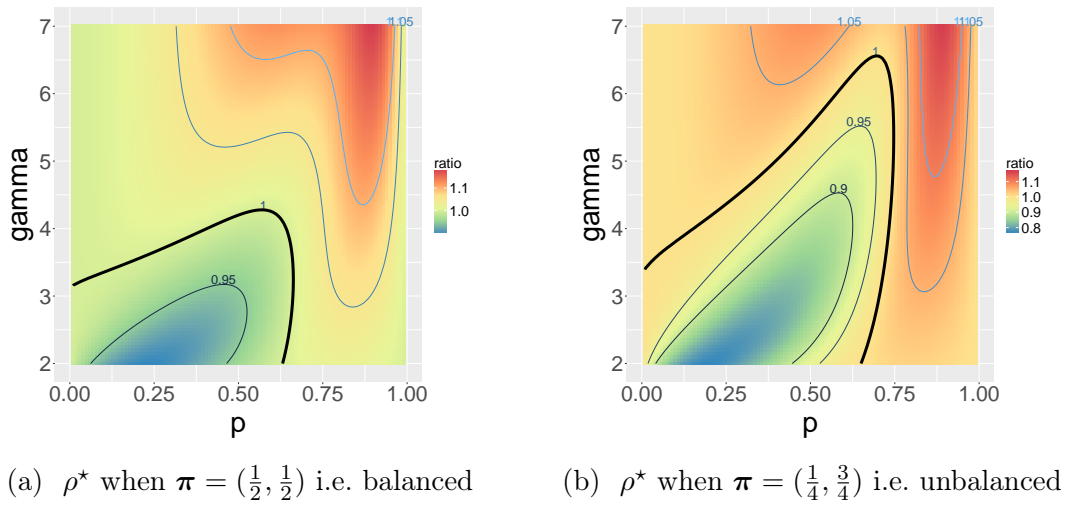


Figure 5: The ratio ρ^* for $p \in (0, 1), \gamma \in [2, 7]$ when $q = p^\gamma$ in Section 5.1.3.

Figure 2 where ASE is preferred.

In Figure 4, the progression from left to right corresponds to tending towards the approximation presented in Eq. (17). For larger values of γ when $q = p^\gamma$ (not shown), the region where ASE > LSE continues to expand. We do not discuss or pursue the taking of limits within the parameter space(s) in light of degenerate boundary value behavior and in order to avoid possible misinterpretation.

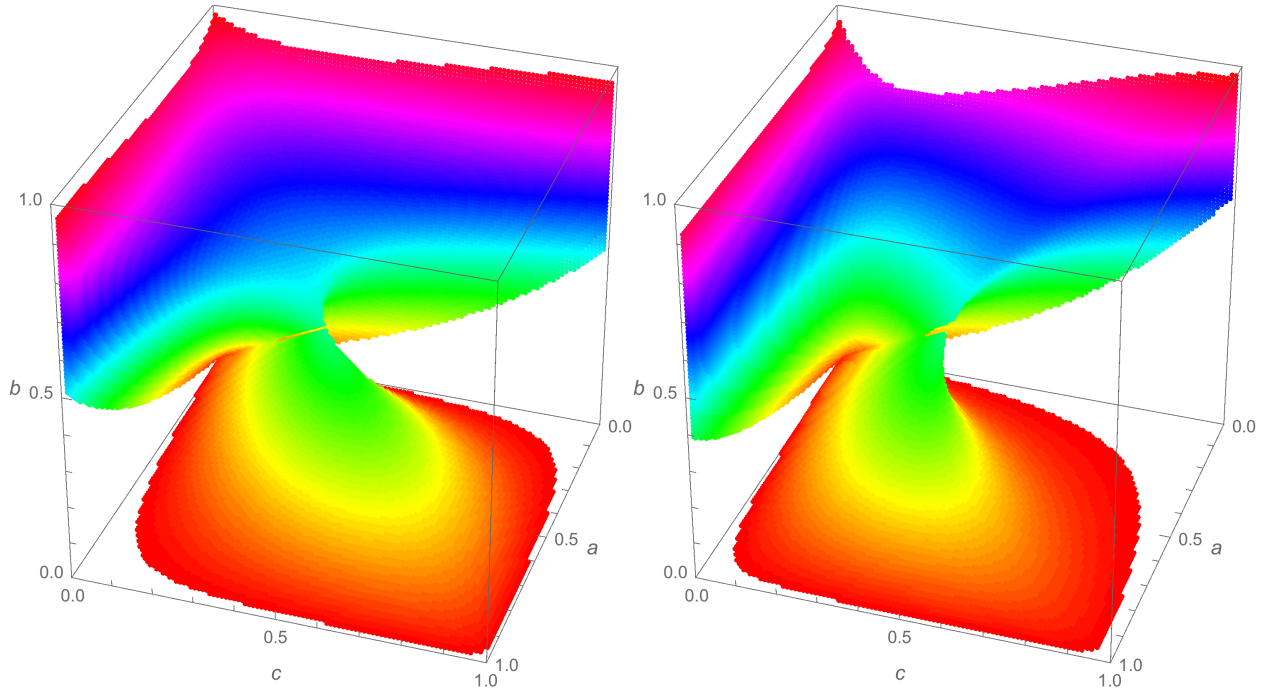
Figure 5 offers a different perspective in which γ is allowed to vary continuously for both the balanced and the unbalanced regime. As in Figure 3, Figure 5 demonstrates that LSE is preferred for network structure wherein the block with comparatively higher edge probability exhibits smaller block membership size.

5.1.4 Full rank two-block stochastic block models

This section presents a macroscopic view of full rank two-block SBMs with $\mathbf{B} = \begin{bmatrix} a & b \\ b & c \end{bmatrix}$, $(a, b, c) \in (0, 1)^3$, for the regimes $\boldsymbol{\pi} = (\frac{1}{2}, \frac{1}{2})$ and $\boldsymbol{\pi} = (\frac{1}{4}, \frac{3}{4})$. The parameter space is partitioned via the latent space geometry of \mathbf{B} , namely according to whether \mathbf{B} is either positive definite or indefinite.

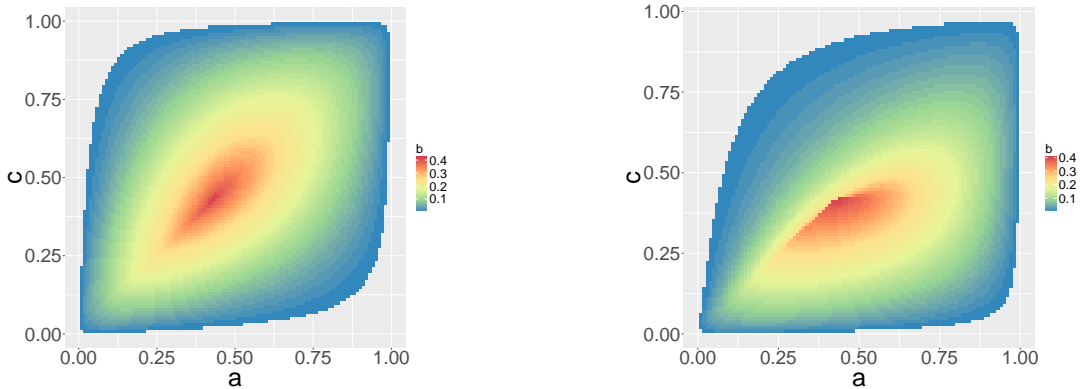
Figure 6a and Figure 6b each present a three-dimensional view of the region in the parameter space where ASE < LSE. The separate positive definite and indefinite parameter regions exhibiting ASE < LSE can be seen extending from faces of the unit cube. Specifically, the conic-like region rising up from the $b = 0$ face corresponds to \mathbf{B} for which $\mathbf{B} \in \mathbb{PD}_2$, whereas the hyperbolic-like regions extending from the $a = 0$ and $c = 0$ faces corresponds to \mathbf{B} for which $\mathbf{B} \in \mathbb{IND}_2$.

For the balanced case reflected in Figure 6a, let $a \geq c$ without loss of generality by symmetry, and hence ρ^* is symmetric about the plane defined by $a = c$. For the unbalanced case shown in Figure 6b, symmetry no longer holds, and geometric warping behavior can be seen with respect to the $a = c$ plane. Figure 7a and Figure 7b provide a birds-eye view of the three-dimensional positive definite parameter region from the vantage point $b = \infty$. The latter



(a) $\rho^* < 1$ for $\text{rank}(\mathbf{B}) = 2$ when $\boldsymbol{\pi} = (\frac{1}{2}, \frac{1}{2})$ (b) $\rho^* < 1$ for $\text{rank}(\mathbf{B}) = 2$ when $\boldsymbol{\pi} = (\frac{1}{4}, \frac{3}{4})$

Figure 6: The parameter region where $\text{ASE} < \text{LSE}$ for full rank \mathbf{B} in Section 5.1.4. The plots depict numerical evaluations of ρ^* for $a, b, c \in [0.01, 0.99]$ with step size 0.01.



(a) $\rho^* < 1$ for $\mathbf{B} \in \mathbb{PD}_2$ when $\boldsymbol{\pi} = (\frac{1}{2}, \frac{1}{2})$ (b) $\rho^* < 1$ for $\mathbf{B} \in \mathbb{PD}_2$ when $\boldsymbol{\pi} = (\frac{1}{4}, \frac{3}{4})$

Figure 7: A top-down projected view of the positive definite region where $\text{ASE} < \text{LSE}$ in Section 5.1.4, with a , b , and c corresponding to length, depth, and width, respectively. The plots depict numerical evaluations of ρ^* for $a, b, c \in [0.01, 0.99]$ with step size 0.01.

provides another view of the warping phenomenon observed for $\boldsymbol{\pi} = (\frac{1}{4}, \frac{3}{4})$ that holds in general for all unbalanced regimes.

In both block size regimes depicted in Figure 6, the colored parameter region occupies less than one-fourth of the unit cube volumetrically, thereby quantitatively providing a coarse overall sense in which ASE is to be preferred to LSE for numerous two-block SBM models.

5.2 The K -block model with homogeneous balanced affinity network structure

This section generalizes the analysis in Section 5.1.1 to the setting of K -block homogeneous balanced affinity SBMs where $\mathbf{B}_{ij} = a$ for all $i = j$, $\mathbf{B}_{ij} = b$ for all $i \neq j$, $0 < b < a < 1$, and $\pi_i = \frac{1}{K}$ for $1 \leq i \leq K$.

Theorem 6. *For K -block homogeneous balanced affinity SBM models as in Section 5.2, the ratio ρ^* in Eq. (12) can be expressed analytically as*

$$\rho^* = 1 + \frac{(a-b)^2(3a(a-1)+3b(b-1)(K-1)+4abK)}{4(a+(K-1)b)^2(a(1-a)+b(1-b))} := 1 + c_{a,b,K} \times \psi_{a,b,K}, \quad (18)$$

where $\psi_{a,b,K} := 3a(a-1) + 3b(b-1)(K-1) + 4abK$ and $c_{a,b,K} > 0$.

As in Table 1, the function $\psi_{a,b,K}$ is the discriminating term that explicitly characterizes the relative performance of ASE and LSE.

Here $\psi_{a,b,K}$ satisfies $(4ab - 3(a - b^2))K < \psi_{a,b,K} < (4ab)K$, and there are explicit constants $c_{a,b}^{(1)}$ and $c_{a,b}^{(2)}$ depending only on a and b such that $\frac{1}{K}c_{a,b}^{(1)} < c_{a,b,K} \times \psi_{a,b,K} < \frac{1}{K}c_{a,b}^{(2)}$. Taking a and b to be fixed, these observations allow Eq. (18) to be summarized in terms of K as

$$\rho^* = 1 + \Theta_{a,b}\left(\frac{1}{K}\right), \quad (19)$$

demonstrating that $\rho^* \rightarrow 1$ as $K \rightarrow \infty$. In words, for the class of SBMs under consideration, ASE and LSE in a sense have asymptotically (in K) equivalent embedding performance (via ρ^*). This amounts to a statement concerning a sequence of models with a necessarily growing number of vertices in order to ensure the underlying assumption of equal block sizes.

Rewriting the level-set $\psi_{a,b,K} = 0$, which holds if and only if $\rho^* = 1$, yields the equation

$$\left(\frac{1-a}{b}\right) \frac{1}{K} + \left(\frac{1-b}{a}\right) \frac{K-1}{K} = \frac{4}{3}, \quad (20)$$

together with the observation that $\text{ASE} > \text{LSE}$ (resp. $\text{ASE} < \text{LSE}$) when the left-hand side of Eq. (20) is less than (resp. greater than) the value $\frac{4}{3}$. The above equation perhaps interestingly depicts a convex combination in K of a reparameterization in terms of the variables $\frac{1-a}{b}$ and $\frac{1-b}{a}$, where the value $\frac{4}{3}$ is interpretable as a Chernoff-based information theoretic threshold.

The observation that $\psi_{a,b,K} > (4ab - 3(a - b^2))K$ in the context of Eq. (18) implies a sufficient condition for determining a parameter region in which $\text{ASE} > \text{LSE}$ *uniformly in* K . Specifically, the condition $(4ab - 3(a - b^2)) > 0$, equivalently written as $\frac{a-b^2}{ab} < \frac{4}{3}$, ensures that $\psi_{a,b,K} > 0$ and hence that $\rho^* > 1$.

Remark 8 (Detectability and phase transitions in random graph models). With respect to the random graph literature, the setting considered in this paper corresponds to a strong consistency regime (i.e. exact recovery) in which the block membership of each individual vertex is recovered almost surely for graphs on n vertices with $n \rightarrow \infty$. For different regimes where edge probabilities are allowed to decrease as a function of n , numerous deep and fascinating detectability and phase transition phenomena are known, some of which also employ Chernoff divergence and related considerations (Abbe, 2018). In the context of homogeneous balanced affinity SBMs, the quantity $\text{SNR} := \frac{(a-b)^2}{K(a+(K-1)b)}$ has been shown to function as an important information-theoretic signal-to-noise ratio. Here too the SNR appears, albeit with respect to $c_{a,b,K}$, in the sense that

$$c_{a,b,K} := \frac{(a-b)^2}{4(a+(K-1)b)^2(a(1-a)+b(1-b))} \equiv \left(\frac{(a-b)^2}{K(a+(K-1)b)}\right) \tilde{c}_{a,b,K}$$

for some constant $\tilde{c}_{a,b,K} > 0$. Perhaps more interestingly,

$$c_{a,b,K} \equiv \frac{1}{4} \left(\frac{\lambda_{\min}(\mathbf{B}(K))}{\lambda_{\max}(\mathbf{B}(K))}\right)^2 \left(\frac{1}{\sigma^2(\mathbf{B}_{11}(K)) + \sigma^2(\mathbf{B}_{12}(K))}\right)$$

where $\sigma^2(\mathbf{B}_{ij}(K))$ is the edge variance corresponding to a pair of vertices in blocks i and j , together with $\lambda_{\min}(\mathbf{B}(K)) = a - b$ and $\lambda_{\max}(\mathbf{B}(K)) = a + (K - 1)b$, noting that the constant factor $\frac{1}{4}$ could just as easily be absorbed by redefining $\psi_{a,b,K}$. It may well prove fruitful to further investigate these observations in light of existing results.

6 Discussion and Conclusions

Loosely speaking, Laplacian spectral embedding may be viewed as a degree-normalized version of adjacency spectral embedding in light of Eq. (3). As such, our analysis complements existing literature that seeks to understand normalization in the context of spectral methods (Sarkar and Bickel, 2015; von Luxburg, 2007). Moreover, our work together with Rubin-Delanchy et al. (2017) addresses network models exhibiting indefinite geometry, an area that has received comparatively limited attention in the statistical network analysis literature. The ability of indefinite modeling considerations to reflect widely-observed disassortative community structure is encouraging and suggests future research activity in this and related directions.

Core-periphery network structure, broadly construed, is demonstrably ubiquitous in real-world networks (Csermely et al., 2013; Holme, 2005; Leskovec et al., 2009). With this understanding and the ability of the SBM to serve as a building block for hierarchically modeling complex network structure, our findings pertaining to spectral embedding for core-periphery structure may be of particular interest.

This paper examines the information-theoretic relationship between the performance of two competing, widely-popular graph embeddings and subsequent vertex clustering with an eye towards underlying network model structure. The findings presented in Section 5 support the claim that, for *sparsity* interpreted as \mathbf{B} having entries that are small, loosely speaking, “Laplacian spectral embedding favors relatively sparse graphs, whereas adjacency spectral embedding favors not-too-sparse graphs.” Moreover, our results provide evidence in support of the claim that “adjacency spectral embedding favors certain core-periphery network structure.” Of course, caution must be exercised when making such general assertions, since the findings in this paper demonstrate intricate and nuanced functional relationships linking spectral embedding performance to network model structure. Nevertheless, we believe such summarative statements are both faithful and useful for conveying a high-level, macroscopic overview of the investigation presented in this work.

Acknowledgments

This work is partially supported by the XDATA and D3M programs of the Defense Advanced Research Projects Agency (DARPA) and by the Acheson J. Duncan Fund for the Advancement of Research in Statistics at Johns Hopkins University. Part of this work was done during visits by JC and CEP to the Isaac Newton Institute for Mathematical Sciences at the University of Cambridge (UK) under EPSCR grant EP/K032208/1. JC thanks Zachary Lubberts for productive discussions.

7 Supplementary material

7.1 Latent position geometry

All stochastic block models in Definition 1 can be formulated as instantiations of generalized random dot product graph models possessing inherent latent position (vector) structure. Earlier observations for the two-block SBM in Section 5 are summarized in the following table, for which the implicit underlying vector $\boldsymbol{\pi}$ may be viewed as an additional parameter space dimension that weights the latent positions ν_1 and ν_2 by π_1 and π_2 , respectively.

Model geometry:	Canonical latent positions:
Positive definite $\mathbf{B}(a, b, c)$	$\nu_1 = (\sqrt{a}, 0), \nu_2 = (b/\sqrt{a}, \sqrt{ac - b^2}/\sqrt{a})$ in \mathbb{R}^2
Indefinite $\mathbf{B}(a, b, c)$	$\nu_1 = (\sqrt{a}, 0), \nu_2 = (b/\sqrt{a}, \sqrt{b^2 - ac}/\sqrt{a})$ in \mathbb{R}^2
Rank one $\mathbf{B}(p^2, pq, q^2)$	$\nu_1 = p, \nu_2 = q$ in \mathbb{R}

For the homogeneous balanced affinity two-block network structure investigated in Section 5.1.1, the latent position geometry can be equivalently reparameterized as two vectors on the circle of radius $r := \sqrt{a}$ separated by the angle $\theta := \arccos(b/a)$. This behavior generalizes to the homogeneous balanced affinity K -block model.

When $\mathbf{B} \equiv \mathbf{B}(K) \in (0, 1)^{K \times K}$ has value a on the main diagonal and value b on the off-diagonal with $0 < b < a < 1$, we can write $\mathbf{B} = \mathbf{X}\mathbf{X}^\top$ via the Cholesky decomposition, where \mathbf{X} has rows given by $\mathbf{X} = [x_1 | x_2 | \dots | x_K]^\top$. For each $i \in [K]$ let the zero-dilation of the \mathbb{R}^K vector x_i be denoted by $x_i^\circ := (x_i, 0) \in \mathbb{R}^{K+1}$. For $K = 2, 3, 4$, \mathbf{X} is given by

$$\mathbf{X}(2) := \begin{bmatrix} \sqrt{a} & 0 \\ \frac{b}{\sqrt{a}} & \sqrt{\frac{(a-b)(a+b)}{a}} \end{bmatrix}, \quad (21)$$

$$\mathbf{X}(3) := \begin{bmatrix} \sqrt{a} & 0 & 0 \\ \frac{b}{\sqrt{a}} & \sqrt{\frac{(a-b)(a+b)}{a}} & 0 \\ \frac{b}{\sqrt{a}} & \sqrt{\frac{(a-b)(a+b)}{a}} \frac{b}{a+b} & \sqrt{\frac{(a-b)(a+2b)}{a+b}} \end{bmatrix}, \quad (22)$$

$$\mathbf{X}(4) := \begin{bmatrix} \sqrt{a} & 0 & 0 & 0 \\ \frac{b}{\sqrt{a}} & \sqrt{\frac{(a-b)(a+b)}{a}} & 0 & 0 \\ \frac{b}{\sqrt{a}} & \sqrt{\frac{(a-b)(a+b)}{a}} \frac{b}{a+b} & \sqrt{\frac{(a-b)(a+2b)}{a+b}} & 0 \\ \frac{b}{\sqrt{a}} & \sqrt{\frac{(a-b)(a+b)}{a}} \frac{b}{a+b} & \sqrt{\frac{(a-b)(a+2b)}{a+b}} \frac{b}{a+2b} & \sqrt{\frac{(a-b)(a+3b)}{a+2b}} \end{bmatrix}. \quad (23)$$

By induction, for $K \geq 3$, the entries of the vector x_K are given by

$$x_K = \left(x_{K-1}^1, x_{K-1}^2, \dots, x_{K-1}^{K-2}, \left(\frac{b}{a+(K-2)b} \right) x_{K-1}^{K-1}, \sqrt{\frac{(a-b)(a+(K-1)b)}{a+(K-2)b}} \right)^\top \in \mathbb{R}^K. \quad (24)$$

Only \mathbf{I}_0^K and \mathbf{I}_{K-1}^1 are necessary with respect to combining possible inner products on account of the sign-flip involving $a - b$. Beginning with the second row in each of the \mathbf{X} matrices, the first column of each matrix can be written in the more illuminating form $\sqrt{a} \frac{b}{a}$.

For this specific K -block model, symmetry with respect to equally-spaced vectors on the \sqrt{a} -radius sphere in \mathbb{R}^K together with block membership balancedness translates into shared covariance structure such that Eq. (12) reduces to Eq. (13). The first two rows of \mathbf{X} are ideal candidates to serve as canonical latent positions for subsequent computation, since these vectors are maximally sparse in the sense of having the fewest non-zero entries and merely become zero-inflated as a function of K . These geometric considerations are crucial in the subsequent proof of Theorem 6.

7.2 Analytic derivations for the two-block SBM

The value of ρ^* in Eq. (14) for the homogeneous balanced two-block SBM can be computed by brute force; however, such an approach offers only limited insight and understanding of

how the covariance structure in Theorem 4 and Theorem 5 interact to yield differences in relative spectral embedding performance as measured via Chernoff information. This section offers a different approach to understanding ρ^* as a covariance-based spectral quantity.

The following lemma is a general matrix analysis observation that establishes a correspondence between the inverse of a convex combination of 2×2 matrices and the inverses of the original 2×2 matrices. The proof of Lemma 7 follows directly from elementary computations and is therefore omitted. Extending Lemma 7 to $n \times n$ invertible matrices is intractable in general.

Lemma 7. *Let $\mathbf{M}_0, \mathbf{M}_1 \in \mathbb{R}^{2 \times 2}$ be two invertible matrices. For each $t \in [0, 1]$ define the matrix $\mathbf{M}_t := (1 - t)\mathbf{M}_0 + t\mathbf{M}_1$. Provided \mathbf{M}_t is invertible, then the inverse matrix \mathbf{M}_t^{-1} can be expressed as*

$$\mathbf{M}_t^{-1} \equiv \frac{(1-t)\mathbf{M}_0^{-1} + \det(\mathbf{M}_1\mathbf{M}_0^{-1})t\mathbf{M}_1^{-1}}{\det(\mathbf{M}_1\mathbf{M}_0^{-1})t^2 + \text{tr}(\mathbf{M}_1\mathbf{M}_0^{-1})t(1-t) + (1-t)^2}. \quad (25)$$

If, in the context of Lemma 7, $\det(\mathbf{M}_1\mathbf{M}_0^{-1}) = 1$, then Eq. (25) simplifies to

$$\mathbf{M}_t^{-1} \equiv \frac{(1-t)\mathbf{M}_0^{-1} + t\mathbf{M}_1^{-1}}{t^2 + \text{tr}(\mathbf{M}_1\mathbf{M}_0^{-1})t(1-t) + (1-t)^2},$$

which is nearly a convex combination of the inverse matrices \mathbf{M}_0^{-1} and \mathbf{M}_1^{-1} modulo division by a degree two polynomial in the parameter t . If, in addition, $\text{tr}(\mathbf{M}_1\mathbf{M}_0^{-1}) \neq -2$ (which always holds when \mathbf{M}_0 and \mathbf{M}_1 are both positive definite), then the inverse matrix at the value $t = \frac{1}{2}$ further simplifies to

$$\mathbf{M}_{1/2}^{-1} \equiv \left(\frac{2}{2 + \text{tr}(\mathbf{M}_1\mathbf{M}_0^{-1})} \right) (\mathbf{M}_0^{-1} + \mathbf{M}_1^{-1}). \quad (26)$$

For the homogeneous balanced two-block SBM considered in Section 5.1.1, one can explicitly check that the above $\det(\cdot)$ and $\text{tr}(\cdot)$ conditions are satisfied. Moreover, the value $t^* = \frac{1}{2}$ achieves the supremum in both the numerator and denominator of ρ^* in Eq. (12). With these observations in hand, it follows by subsequent computations that for both the positive definite and indefinite regimes,

$$\begin{aligned}
\rho^* &= \frac{\|\nu_1 - \nu_2\|_{\Sigma_{1,2}^{-1}(1/2)}^2}{\|\tilde{\nu}_1 - \tilde{\nu}_2\|_{\tilde{\Sigma}_{1,2}^{-1}(1/2)}^2} \\
&= \left(\frac{\left(\frac{2}{2 + \text{tr}(\Sigma(\nu_1)\Sigma^{-1}(\nu_2))} \right)}{\left(\frac{2}{2 + \text{tr}(\tilde{\Sigma}(\nu_1)\tilde{\Sigma}^{-1}(\nu_2))} \right)} \right) \times \left(\frac{(\nu_1 - \nu_2)^\top (\Sigma^{-1}(\nu_1) + \Sigma^{-1}(\nu_2))(\nu_1 - \nu_2)}{(\tilde{\nu}_1 - \tilde{\nu}_2)^\top (\tilde{\Sigma}^{-1}(\nu_1) + \tilde{\Sigma}^{-1}(\nu_2))(\tilde{\nu}_1 - \tilde{\nu}_2)} \right) \\
&= \left(\frac{2 + \text{tr}(\tilde{\Sigma}(\nu_1)\tilde{\Sigma}^{-1}(\nu_2))}{2 + \text{tr}(\Sigma(\nu_1)\Sigma^{-1}(\nu_2))} \right) \times 1 \\
&= 1 + \frac{\text{tr}(\tilde{\Sigma}(\nu_1)\tilde{\Sigma}^{-1}(\nu_2)) - \text{tr}(\Sigma(\nu_1)\Sigma^{-1}(\nu_2))}{2 + \text{tr}(\Sigma(\nu_1)\Sigma^{-1}(\nu_2))} \\
&= 1 + \frac{(a-b)^2(3a(a-1) + 3b(b-1) + 8ab)}{4(a+b)^2(a(1-a) + b(1-b))}.
\end{aligned}$$

7.3 Proof of Theorem 6

This section is dedicated to proving Theorem 6 for $K \geq 2$ block SBMs exhibiting homogeneous balanced affinity structure. The proof is divided into two parts which separately evaluate the suprema in the numerator and denominator of ρ^* in Eq. (12). By invoking underlying symmetries in latent space and the covariance structure of the ASE and LSE limit results, respectively, we shall leverage the (considerably simpler) ASE computations (numerator) when working with LSE (denominator). Simplifying the numerator and denominator yields the more easily interpretable (shifted) expression of ρ^* provided in Eq. (18).

Proof: First recall the discussion of latent space geometry in Section 7.1, specifically that for the homogeneous balanced affinity K -block SBM, the canonical latent positions can be arranged row-wise as a lower-triangular matrix \mathbf{X} where each latent position vector has norm \sqrt{a} and each pair of distinct latent position vectors has common inner-product b . This rotational symmetry implies rotational symmetry for the block-conditional covariance matrices in Theorems 4–5, and as such, the formulation of ρ^* in Eq. (18) can be reduced to simply working with the latent position pair $\{\nu_1, \nu_2\}$ without loss of generality. This pair is attractive, since the non-zero entries of these vectors remain unchanged for all $K \geq 2$. One need only work with the standard inner product since $d^- = 0$.

7.3.1 Proof of Theorem 6: ASE (numerator)

Let $g(x, X_1) := \langle x, X_1 \rangle (1 - \langle x, X_1 \rangle)$ and for $0 < t < 1$ define $g_t(x_1, x_2, X_1) := tg(x_1, X_1) + (1-t)g(x_2, X_1)$. By Theorem 4, $\Sigma(x) = \Delta^{-1} \mathbb{E}[g(x, X_1) X_1 X_1^\top] \Delta^{-1}$, and therefore $\Sigma_{1,2}(t) := t\Sigma(\nu_1) + (1-t)\Sigma(\nu_2) = \Delta^{-1} \mathbb{E}[g_t(\nu_1, \nu_2, X_1) X_1 X_1^\top] \Delta^{-1}$. Evaluating the inner expectation yields

$$\begin{aligned} \mathbb{E}[g_t(\nu_1, \nu_2, X_1) X_1 X_1^\top] &= \sum_{i=1}^K \frac{1}{K} (t \langle \nu_1, \nu_i \rangle (1 - \langle \nu_1, \nu_i \rangle) + (1-t) \langle \nu_2, \nu_i \rangle (1 - \langle \nu_2, \nu_i \rangle)) \nu_i \nu_i^\top \\ &= b(1-b) \Delta + \left(\frac{a(1-a) - b(1-b)}{K} \right) [t \nu_1 \nu_1^\top + (1-t) \nu_2 \nu_2^\top] \\ &= b(1-b) \Delta + \mathbf{V} (c_0 \mathbf{D}_t) \mathbf{V}^\top, \end{aligned}$$

where $\mathbf{V} := [\nu_1 | \nu_2] \in \mathbb{R}^{K \times 2}$, $c_0 := \left(\frac{a(1-a) - b(1-b)}{K} \right)$, and $\mathbf{D}_t := \text{diag}(t, 1-t)$. Clearly $c_0 \mathbf{D}_t$ is invertible, as is Δ since the underlying distribution F is non-degenerate. Moreover, \mathbf{X} is also invertible since the K -block model under consideration is also rank K . The relation $\mathbf{X}^\top \mathbf{X} = K \Delta$ implies $\Delta^{-1} = K \mathbf{X}^{-1} (\mathbf{X}^\top)^{-1}$ and therefore $\mathbf{X} \Delta^{-1} \mathbf{X}^\top = K \mathbf{I}$, so $\nu_i^\top \Delta^{-1} \nu_j = K \mathbb{I}_{ij}$ where \mathbb{I}_{ij} denotes the indicator function for indices i and j . Thus, $(c_0 \mathbf{D}_t)^{-1} + \frac{1}{b(1-b)} \mathbf{V}^\top \Delta^{-1} \mathbf{V} = (c_0 \mathbf{D}_t)^{-1} + \frac{K}{b(1-b)} \mathbf{I}$, which is also invertible. By an application of the Sherman–Morrison–Woodbury matrix inversion formula (Horn and Johnson (2012), Section 0.7.4), then

$$\begin{aligned} \mathbb{E}[g_t(\nu_1, \nu_2, X_1) X_1 X_1^\top]^{-1} &= (b(1-b) \Delta + \mathbf{V} (c_0 \mathbf{D}_t) \mathbf{V}^\top)^{-1} \\ &= \left(\frac{1}{b(1-b)} \right) \Delta^{-1} - \left(\frac{1}{b(1-b)} \right)^2 \Delta^{-1} \mathbf{V} \left(\frac{1}{c_0} \mathbf{D}_t^{-1} + \frac{K}{b(1-b)} \mathbf{I} \right)^{-1} \mathbf{V}^\top \Delta^{-1}. \end{aligned}$$

For $\nu := \nu_1 - \nu_2 = \left(\frac{a-b}{\sqrt{a}}, -\sqrt{\frac{(a-b)(a+b)}{a}}, 0, \dots, 0 \right)^\top \in \mathbb{R}^K$, then $\nu^\top \Delta \nu = \frac{2}{K} (a-b)^2$ and $\mathbf{V}^\top \nu = (a-b)(1, -1)^\top \in \mathbb{R}^2$. These observations together with subsequent computations yield the following chain of equalities.

$$\begin{aligned}
\|\nu\|_{\Sigma_{1,2}^{-1}(t)}^2 &= \nu^\top (\Delta^{-1} \mathbb{E}[g_t(\nu_1, \nu_2, X_1) X_1 X_1^\top] \Delta^{-1})^{-1} \nu \\
&= \nu^\top (\Delta \mathbb{E}[g_t(\nu_1, \nu_2, X_1) X_1 X_1^\top]^{-1} \Delta) \nu \\
&= \nu^\top \Delta \left(\frac{1}{b(1-b)} \Delta^{-1} - \left(\frac{1}{b(1-b)} \right)^2 \Delta^{-1} \mathbf{v} \left(\frac{1}{c_0} \mathbf{D}_t^{-1} + \frac{K}{b(1-b)} \mathbf{I} \right)^{-1} \mathbf{v}^\top \Delta^{-1} \right) \Delta \nu \\
&= \nu^\top \left(\frac{1}{b(1-b)} \Delta - \left(\frac{1}{b(1-b)} \right)^2 \mathbf{v} \left(\frac{1}{c_0} \mathbf{D}_t^{-1} + \frac{K}{b(1-b)} \mathbf{I} \right)^{-1} \mathbf{v}^\top \right) \nu \\
&= \left(\frac{1}{b(1-b)} \right) \nu^\top \Delta \nu - \left(\frac{1}{b(1-b)} \right)^2 \nu^\top \mathbf{v} \left(\frac{1}{c_0} \mathbf{D}_t^{-1} + \frac{K}{b(1-b)} \mathbf{I} \right)^{-1} \mathbf{v}^\top \nu \\
&= \left(\frac{2(a-b)^2}{b(1-b)K} \right) - \left(\frac{a-b}{b(1-b)} \right)^2 (1, -1) \left(\frac{1}{c_0} \mathbf{D}_t^{-1} + \frac{K}{b(1-b)} \mathbf{I} \right)^{-1} (1, -1)^\top \\
&= \left(\frac{2(a-b)^2}{b(1-b)K} \right) - \left(\frac{a-b}{b(1-b)} \right)^2 \text{tr} \left(\left(\frac{1}{c_0} \mathbf{D}_t^{-1} + \frac{K}{b(1-b)} \mathbf{I} \right)^{-1} \right) \\
&= \left(\frac{2(a-b)^2}{b(1-b)K} \right) - \left(\frac{a-b}{b(1-b)} \right)^2 \left(\frac{(a(1-a)-b(1-b))b(1-b)t}{((a(1-a)-b(1-b))t+b(1-b))K} + \frac{(a(1-a)-b(1-b))b(1-b)(1-t)}{((a(1-a)-b(1-b))(1-t)+b(1-b))K} \right) \\
&= \frac{(a-b)^2(a(a-1)+b(b-1))}{(a(1-a)+(a(a-1)-b(b-1))t)(b(b-1)+(a(a-1)-b(b-1))t)K}.
\end{aligned}$$

In particular,

$$\sup_{t \in (0,1)} \left[t(1-t) \|\nu\|_{\Sigma_{1,2}^{-1}(t)}^2 \right] = \frac{1}{K} \frac{(a-b)^2}{a(1-a)+b(1-b)}, \quad (27)$$

where by underlying symmetry the supremum is achieved at $t^* = \frac{1}{2}$ over the entire parameter region $0 < b < a < 1$.

7.3.2 Proof of Theorem 6: LSE (denominator)

Recall that for this model $\mathbf{I}_d^{d^+} \equiv \mathbf{I}_d$ since $d^- = 0$. From Theorem 5 for LSE, the block conditional covariance matrix for each latent position x can be written in the modified form

$$\tilde{\Sigma}(x) = \mathbb{E} \left[\begin{pmatrix} g(x, X_1) \\ \langle x, \mu \rangle \end{pmatrix} \left(\tilde{\Delta}^{-1} X_1 - \frac{x}{2\langle x, \mu \rangle} \right) \left(\tilde{\Delta}^{-1} X_1 - \frac{x}{2\langle x, \mu \rangle} \right)^\top \right].$$

We begin with several preliminary observations in order to define the quantities c_1, c_2 , and

c_3 . Namely, for each latent position (row) x of \mathbf{X} ,

$$\langle x, \mu \rangle = \left(\frac{a+(K-1)b}{K} \right) =: c_1, \quad (28)$$

$$\mathbb{E}[g(x, X_1)] = \left(\frac{a(1-a)+(K-1)b(1-b)}{K} \right) =: c_2, \quad (29)$$

$$\mathbb{E}[g(x, X_1)X_1] := \left(\frac{a(1-a)-b(1-b)}{K} \right) x + b(1-b)\mu =: c_3x + b(1-b)\mu. \quad (30)$$

Subsequent computations yield

$$\begin{aligned} \Delta x &= \left(\frac{a-b}{K} \right) x + b\mu, \\ [\Delta - \left(\frac{a-b}{K} \right) \mathbf{I}] xx^\top &= b\mu x^\top, \\ \langle \Delta x, x \rangle &= \left(\frac{a^2+(K-1)b^2}{K} \right), \\ \tilde{\Delta} &\equiv \mathbb{E} \left[\frac{1}{\langle X_1, \mu \rangle} X_1 X_1^\top \right] = \frac{1}{c_1} \Delta. \end{aligned}$$

The above observations allow us to write $\tilde{\Sigma}(x)$ as

$$\begin{aligned} &\mathbb{E} \left[\left(\frac{g(x, X_1)}{\langle x, \mu \rangle} \right) \left(\frac{\tilde{\Delta}^{-1} X_1}{\langle X_1, \mu \rangle} - \frac{x}{2\langle x, \mu \rangle} \right) \left(\frac{\tilde{\Delta}^{-1} X_1}{\langle X_1, \mu \rangle} - \frac{x}{2\langle x, \mu \rangle} \right)^\top \right] \\ &= \tilde{\Delta}^{-1} \mathbb{E} \left[\frac{g(x, X_1)}{\langle x, \mu \rangle} \left(\frac{X_1}{\langle X_1, \mu \rangle} - \frac{\tilde{\Delta} x}{2\langle x, \mu \rangle} \right) \left(\frac{X_1}{\langle X_1, \mu \rangle} - \frac{\tilde{\Delta} x}{2\langle x, \mu \rangle} \right)^\top \right] \tilde{\Delta}^{-1} \\ &= \frac{1}{c_1} \Delta^{-1} \mathbb{E} \left[g(x, X_1) \left(X_1 - \frac{1}{2c_1} \Delta x \right) \left(X_1 - \frac{1}{2c_1} \Delta x \right)^\top \right] \Delta^{-1}. \end{aligned}$$

Expanding the term inside the expectation and applying linearity of expectation allows us to analyze each piece in turn. The first term in the expansion can be analyzed via the previous computations under ASE. For the second term,

$$\begin{aligned} \mathbb{E} \left[\frac{1}{2c_1} g(x, X_1) X_1 x^\top \Delta \right] &= \frac{1}{2c_1} \mathbb{E}[g(x, X_1) X_1] x^\top \Delta \\ &= \frac{1}{2c_1} (c_3 x x^\top + b(1-b)\mu x^\top) \Delta \\ &= \frac{1}{2c_1} (c_3 x x^\top + (1-b) [\Delta - \left(\frac{a-b}{K} \right) \mathbf{I}] x x^\top) \Delta \\ &= \left(\frac{1-b}{2c_1} \right) \Delta x x^\top \Delta + \left(\frac{Kc_3 - (a-b)(1-b)}{2c_1 K} \right) x x^\top \Delta \\ &= \left(\frac{1-b}{2c_1} \right) \Delta x x^\top \Delta + \left(\frac{a(b-a)}{2c_1 K} \right) x x^\top \Delta. \end{aligned}$$

Note that the transpose of this matrix corresponds to the third term in the implicit expansion of interest (not shown). Finally, the fourth term simply reduces to the form

$$\mathbb{E} \left[g(x, X_1) \left(\frac{1}{2c_1} \Delta x \right) \left(\frac{1}{2c_1} \Delta x \right)^\top \right] = c_2 \left(\frac{1}{2c_1} \Delta x \right) \left(\frac{1}{2c_1} \Delta x \right)^\top = \left(\frac{c_2}{4c_1^2} \right) \Delta x x^\top \Delta.$$

Thus,

$$\begin{aligned}
& \mathbb{E} \left[g(x, X_1) \left(X_1 - \frac{1}{2c_1} \Delta x \right) \left(X_1 - \frac{1}{2c_1} \Delta x \right)^\top \right] \\
&= \mathbb{E}[g(x, X_1) X_1 X_1^\top] - \mathbb{E}[\frac{1}{2c_1} g(x, X_1) X_1 x^\top \Delta] - \mathbb{E}[\frac{1}{2c_1} g(x, X_1) X_1 x^\top \Delta]^\top + \mathbb{E}[g(x, X_1) (\frac{1}{2c_1} \Delta x) (\frac{1}{2c_1} \Delta x)^\top] \\
&= \mathbb{E}[g(x, X_1) X_1 X_1^\top] - \left(\frac{a(b-a)}{2c_1 K} \right) x x^\top \Delta - \left(\frac{a(b-a)}{2c_1 K} \right) \Delta x x^\top + \left(\frac{c_2}{4c_1^2} - \frac{1-b}{c_1} \right) \Delta x x^\top \Delta.
\end{aligned}$$

Let $\mathbf{M}_1 \equiv \mathbf{M}_1(t) := \mathbf{V} \mathbf{D}_t \mathbf{V}^\top$ and $\mathbf{M}_2 := \Delta$ with respect to the notation introduced earlier in the derivation for ASE. By completing the appropriate matrix product, there are explicit constants $\{d_i\}_{i=1}^4$ depending on a , b , and K , such that

$$\begin{aligned}
\tilde{\Sigma}_{1,2}(t) &= t \tilde{\Sigma}(\nu_1) + (1-t) \tilde{\Sigma}(\nu_2) \\
&= \Delta^{-1} (d_1 \Delta + d_2 \mathbf{V} \mathbf{D}_t \mathbf{V}^\top + d_3 \mathbf{V} \mathbf{D}_t \mathbf{V}^\top \Delta + d_3 \Delta \mathbf{V} \mathbf{D}_t \mathbf{V}^\top + d_4 \Delta \mathbf{V} \mathbf{D}_t \mathbf{V}^\top \Delta) \Delta^{-1} \\
&= \Delta^{-1} ([d_1 \mathbf{M}_2 + d_5 \mathbf{M}_1] + (\mathbf{I} + d_6 \mathbf{M}_2)(d_7 \mathbf{M}_1)(\mathbf{I} + d_6 \mathbf{M}_2)) \Delta^{-1} \\
&=: \Delta^{-1} (\mathbf{M}_3 + \mathbf{M}_4) \Delta^{-1},
\end{aligned}$$

where $\mathbf{M}_3 \equiv \mathbf{M}_3(t) := d_1 \mathbf{M}_2 + d_5 \mathbf{M}_1(t)$ and $\mathbf{M}_4 \equiv \mathbf{M}_4(t) = (\mathbf{I} + d_6 \mathbf{M}_2)(d_7 \mathbf{M}_1(t))(\mathbf{I} + d_6 \mathbf{M}_2)$.

Note that $\tilde{\nu}_k := \left(\frac{1}{\langle \nu_k, \mu \rangle} \right)^{1/2} \times \nu_k = \left(\frac{K}{a+(K-1)b} \right)^{1/2} \times \nu_k$ for $k = 1, 2$, so

$$\|\tilde{\nu}\|_{\tilde{\Sigma}_{1,2}^{-1}(t)}^2 = \tilde{\nu}^\top \tilde{\Sigma}_{1,2}^{-1}(t) \tilde{\nu} = \left(\frac{K}{a+(K-1)b} \right) \nu^\top \Delta (\mathbf{M}_3 + \mathbf{M}_4)^{-1} \Delta \nu.$$

The above matrix inversion can again be carried out via the Sherman–Morrison–Woodbury formula. We omit the algebraic details. Subsequent computations and simplification yield

$$\sup_{t \in (0,1)} \left[t(1-t) \|\tilde{\nu}\|_{\tilde{\Sigma}_{1,2}^{-1}(t)}^2 \right] = \frac{4(a-b)^2(a+(K-1)b)^2}{4(a(1-a)+b(1-b))(a+(K-1)b)^2 K + (a-b)^2 K(3a(a-1)+3b(b-1)(K-1)+4abK)} \quad (31)$$

where by underlying symmetry the supremum is achieved at $t^* = \frac{1}{2}$ over the entire parameter region $0 < b < a < 1$. Taken together, Eq. (27) and Eq. (31) simplify to yield ρ^* as in Eq. (18), thereby completing the proof. \square

References

- Abbe, E. (2018). Community detection and stochastic block models: Recent developments. *Journal of Machine Learning Research* 18(177), 1–86. [4](#), [5](#), [25](#)
- Airoldi, E. M., D. M. Blei, S. E. Fienberg, and E. P. Xing (2008). Mixed membership stochastic blockmodels. *Journal of Machine Learning Research* 9, 1981–2014. [4](#)
- Athreya, A., D. E. Fishkind, M. Tang, C. E. Priebe, Y. Park, J. T. Vogelstein, K. Levin, V. Lyzinski, Y. Qin, and D. L. Sussman (2018). Statistical inference on random dot product graphs: A survey. *Journal of Machine Learning Research* 18(226), 1–92. [4](#), [7](#)
- Athreya, A., C. E. Priebe, M. Tang, V. Lyzinski, D. J. Marchette, and D. L. Sussman (2016). A limit theorem for scaled eigenvectors of random dot product graphs. *Sankhya A* 78(1), 1–18. [4](#)
- Bhatia, R. (1997). *Matrix Analysis, Volume 169 of Graduate Texts in Mathematics*. Springer-Verlag, New York.
- Bollobás, B., S. Janson, and O. Riordan (2007). The phase transition in inhomogeneous random graphs. *Random Structures and Algorithms* 31(1), 3–122. [3](#)
- Chernoff, H. (1952). A measure of asymptotic efficiency for tests of a hypothesis based on the sum of observations. *The Annals of Mathematical Statistics* 23(4), 493–507. [4](#), [11](#)
- Chernoff, H. (1956). Large-sample theory: Parametric case. *The Annals of Mathematical Statistics* 27(1), 1–22. [11](#)
- Csermely, P., A. London, L.-Y. Wu, and B. Uzzi (2013). Structure and dynamics of core-periphery networks. *Journal of Complex Networks* 1(2), 93–123. [26](#)
- Devroye, L., L. Györfi, and G. Lugosi (2013). *A Probabilistic Theory of Pattern Recognition*, Volume 31. Springer. [12](#)
- Erdős, P. and A. Rényi (1959). On random graphs. *Publicationes Mathematicae (Debrecen)* 6, 290–297. [3](#)

- Fishkind, D. E., D. L. Sussman, M. Tang, J. T. Vogelstein, and C. E. Priebe (2013). Consistent adjacency-spectral partitioning for the stochastic block model when the model parameters are unknown. *SIAM Journal on Matrix Analysis and Applications* 34(1), 23–39. 4
- Hoff, P. D., A. E. Raftery, and M. S. Handcock (2002). Latent space approaches to social network analysis. *Journal of the American Statistical Association* 97(460), 1090–1098. 4
- Holland, P. W., K. B. Laskey, and S. Leinhardt (1983). Stochastic blockmodels: First steps. *Social Networks* 5(2), 109–137. 2
- Holme, P. (2005). Core-periphery organization of complex networks. *Physical Review E* 72, 046111. 26
- Horn, R. A. and C. R. Johnson (2012). *Matrix Analysis*. Cambridge University Press. 32
- Karrer, B. and M. E. J. Newman (2011). Stochastic blockmodels and community structure in networks. *Physical Review E* 83, 016107. 4
- Lei, J. and A. Rinaldo (2015). Consistency of spectral clustering in stochastic block models. *The Annals of Statistics* 43(1), 215–237. 4
- Leskovec, J., K. J. Lang, A. Dasgupta, and M. W. Mahoney (2009). Community structure in large networks: Natural cluster sizes and the absence of large well-defined clusters. *Internet Mathematics* 6(1), 29–123. 26
- Liese, F. and I. Vajda (2006). On divergences and informations in statistics and information theory. *IEEE Transactions on Information Theory* 52(10), 4394–4412. 12
- Lyzinski, V., M. Tang, A. Athreya, Y. Park, and C. E. Priebe (2017). Community detection and classification in hierarchical stochastic blockmodels. *IEEE Transactions on Network Science and Engineering* 4(1), 13–26. 7
- McSherry, F. (2001). Spectral partitioning of random graphs. *In Proceedings of the 42nd IEEE Symposium on Foundations of Computer Science*, 529–537. 4

- Nickel, C. L. M. (2006). Random dot product graphs: A model for social networks. *Ph.D. thesis, Johns Hopkins University*. 4, 7
- Rohe, K., S. Chatterjee, and B. Yu (2011). Spectral clustering and the high-dimensional stochastic block model. *The Annals of Statistics* 39(4), 1878–1915. 4
- Rubin-Delanchy, P., C. E. Priebe, M. Tang, and J. Cape (2017). A statistical interpretation of spectral embedding: the generalised random dot product graph. *arXiv preprint arXiv:1709.05506*. 5, 7, 10, 26
- Sarkar, P. and P. J. Bickel (2015). Role of normalization in spectral clustering for stochastic blockmodels. *The Annals of Statistics* 43(3), 962–990. 4, 26
- Sussman, D. L., M. Tang, D. E. Fishkind, and C. E. Priebe (2014). A consistent adjacency spectral embedding for stochastic blockmodel graphs. *Journal of the American Statistical Association* 107(499), 1119–1128. 4
- Tang, M., A. Athreya, D. L. Sussman, V. Lyzinski, Y. Park, and C. E. Priebe (2017). A semiparametric two-sample hypothesis testing problem for random graphs. *Journal of Computational and Graphical Statistics* 26(2), 344–354. 7
- Tang, M., A. Athreya, D. L. Sussman, V. Lyzinski, and C. E. Priebe (2017). A nonparametric two-sample hypothesis testing problem for random graphs. *Bernoulli* 23(3), 1599–1630. 7
- Tang, M. and C. E. Priebe (2016). Limit theorems for eigenvectors of the normalized Laplacian for random graphs. *arXiv preprint arXiv:1607.0123*, *The Annals of Statistics*, *accepted*. 4, 5, 6, 8, 12
- von Luxburg, U. (2007). A tutorial on spectral clustering. *Statistics and Computing* 17(4), 395–416. 3, 26
- Young, S. and E. Scheinerman (2007). Random dot product graph models for social networks. *Algorithms and Models for the Web-Graph 4863*, 138–149. 4, 7